Facies and evolution of the carbonate factory during the Permian-Triassic crisis in South Tibet, China

Mingtao Li*, **Haijun Song***, **Adam D. Woods†**, **Xu Dai***, **Paul B. Wignall‡**

*****State Key Laboratory of Biogeology and Environmental Geology, School of Earth Sciences, China University of Geosciences, Wuhan 430074, China (E-mail: haijunsong@cug.edu.cn)

†Department of Geological Sciences, California State University, Fullerton, 800N. State College Blvd., Fullerton, CA 92834-6850, USA

‡School of Earth and Environment, University of Leeds, Leeds, LS2 9JT, United Kingdom

ABSTRACT

The nature of Phanerozoic carbonate factories is strongly controlled by the composition of carbonate-producing faunas. During the Permian-Triassic mass extinction (PTME) interval there was a major change in tropical shallow platform facies: Upper Permian bioclastic limestones are characterized by benthic communities with significant richness, e.g., calcareous algae, fusulinids, brachiopods, corals, mollusks, and sponges, while lowermost Triassic carbonates shift to dolomicrite- and bacteria-dominated microbialites in the immediate aftermath of the PTME. However, the spatial-temporal pattern of carbonates distribution in high latitude regions in response to the PTME has received little attention. Facies and evolutionary patterns of a carbonate factory from the northern margin of peri-Gondwana (palaeolatitude ~40° S) are presented here based on four Permian-Triassic boundary sections that span proximal, inner to distal, and outer ramp settings from South Tibet. The results show that a cool-water bryozoan- and echinoderm-dominated carbonate ramp developed in the Late Permian in South Tibet. This was replaced abruptly, immediately after the PTME, by a benthic automicrite factory with minor amounts of calcifying metazoans developed in an inner/middle ramp setting, accompanied by transient subaerial exposure. Subsequently, an extensive homoclinal carbonate ramp developed in South Tibet in the Early Triassic, which mainly consists of homogenous dolomitic lime mudstone/wackestone that lacks evidence of metazoan frame-builders. The sudden transition from a cool-water, heterozoan dominated carbonate ramp to a warm-water, metazoan-free, homoclinal carbonate ramp following the PTME was the result of the combination of the loss of metazoan reef/mound builders, rapid sea level changes across PTME and profound global warming during the Early Triassic.

Keywords: South Tibet, carbonate factory, microfacies, regression, Permian-Triassic mass extinction.

INTRODUCTION

Carbonate factory transitions are usually driven by biotic evolution (Burchette & Wright, 1992; Kiessling et al., 2003; Pomar & Hallock, 2008). Carbonate factories have evolved from microbially-dominated carbonate ramps that were present during the Precambrian (Grotzinger & Knoll, 1999; Cozzi et al., 2004), to microbe-sponge carbonate ramps during the Paleozoic, to Mesozoic platforms dominated by oolites and neritic lime-mud (sourced from phytoplankton and microbial photosynthesis) to Cenozoic skeletal shelves (Kiessling et al., 2003; Pomar & Hallock, 2008).

There were several specific intervals during the evolution of carbonate factories that record abrupt changes in the composition of carbonate producers as the result of mass extinctions (Raup & Sepkoski, 1982). For example, the Permian-Triassic mass extinction (PTME), the most severe biotic crisis of the Phanerozoic, is characterized by a loss of over 90% of marine species, including most carbonate-producing metazoan faunas (Erwin, 1994; Song et al., 2013). The aftermath of this crisis is marked by a variety of anachronistic facies that are typical features of Precambrian carbonate factories (Grotzinger & Knoll, 1999; Sepkoski et al., 1991; Thomson et al., 2014). They include widespread microbialites (Kershaw et al., 1999; Lehrmann, 1999; Baud et al., 2007; Woods, 2014), and seafloor carbonate precipitates (Woods et al., 1999; Baud et al., 2007; Pruss et al., 2008; Woods, 2009; Heindel et al., 2015; Li et al., 2018a). The widespread microbialites are often attributed to blooms of bacteria due to a decline in grazing pressure from metazoans (Schubert & Bottjer, 1992; Xie et al., 2010; Woods, 2014) and/or from the unusual ocean chemistry of the Early Triassic (e.g., Grotzinger and Knoll, l995; Woods, et al., 1999). Overall, the carbonate factory immediately after the PTME shows similarities to that of the Precambrian, and, accordingly, a "benthic-automicrite carbonate factory" model was proposed to provide new insight into carbonate evolution (Pomar & Hallock, 2008). However, most documented anachronistic facies are found in subtropical to tropical shallow-water settings, and the reaction of the deeper-water carbonate factory in high latitude regions is poorly known.

A series of deep-water, Permian-Triassic boundary (PTB) outcrops are exposed in South Tibet (China), providing a unique opportunity to reconstruct a Late Permian to Early Triassic carbonate factory. More than one hundred samples were extracted from these four sections and cut into thin-sections to perform microfacies analysis. This study aims to provide a detailed analysis of the sedimentary transition during the PTME, and explore how the deeper-water carbonate factory in high latitude regions operated in response to the PTME.

GEOLOGICAL SETTING

South Tibet is located within the Tethyan Himalayas (Fig. 1A), and is separated from the Lhasa Block by the Indus-Tsangbo suture to the north, and the High Himalaya, which mainly consist of Precambrian crystalline rocks, to the south (Fig. 1B). The Lhasa Block, which was part of the Gondwana supercontinent and now belongs to the Eurasian plate, began to separate from Gondwana and drift northwards as the Neo-Tethys opened at the end of the Paleozoic (Liu & Einsele, 1994). A broad, passive margin with a slow subsidence rate developed on the northern margin of peri-Gondwana during the initial breakup of Gondwana (Liu & Einsele, 1994), and extensive dolomitic wackestone with sparse pelagic bivalves, crinoids and ostracods was deposited (Garzanti et al., 1994, 1998). Sections from South Tibet (China), Spiti (India) (Ghosh et al., 2016), Manang (Nepal) (Garzanti et al., 1994; Yoshida et al., 2014) and the Salt Range (Pakistan) (Hermann et al., 2012) provide data to reconstruct the sedimentary framework of the northern margin of peri-Gondwana.

Our study area is located in the middle Tethyan Himalaya (Fig. 1B) and has been affected by intense tectonism during the collision of Indian and Asia. This resulted in an irregular and discontinuous distribution of Paleozoic strata. In this study, four sections (i.e., Gongpu, Selong, Tulong, and Qubu) that are exposed along the southern margin of the Tethys Himalaya region (Fig. 1B) were investigated.

Palaeogeographically, the Tethyan Himalaya was located on the northern margin of peri-Gondwana during the Late Permian, with a palaeolatitude of ~40˚S (Fig. 1C). Cool waters are inferred from the occurrence of typical Late Permian cold-water brachiopods, including Taeniothaerus and Trigonotreta and the large, thick-shelled Spiriferella and

Neospirifer brachiopods (Shen et al., 2006). A rapid, global regression occurred at the end of the Permian, which was accompanied by sudden warming, and resulted in the establishment of a warm-water biotic assemblage characterized by abundant conodonts and the occurrence of calcareous sponges (Shen et al., 2003a,b; Wignall & Newton, 2003).

BIOSTRATIGRAPHIC CONTROL

The lithology and stratigraphy of the sections in South Tibet are readily correlated using well-constrained conodont and ammonoid biozones (Fig. 2).

The Selong section is located at Selong village, 77 km NW of the capital of old Tingri County. Detailed conodont biostratigraphy has been carried out and a high-resolution biostratigraphic framework has been established there (Orchard et al., 1994; Wang et al., 2017; Yuan et al., 2018). The 24 m – thick, uppermost Permian Selong Group (Lopingian in age) can be divided into a lower bioclastic rudstone intercalated with dark grey silty shale and an upper, massive crinoid grainstone. The occurrence of the Chonetella nasuta brachiopod Assemblage in the lower units suggests a Wuchiapingian age (Shen et al., 2000), and the occurrence of the conodonts Mesogondolella hendersoni and Mesogondolella sheni in the upper unit indicates a latest Changhsingian age (Yuan et al., 2018). The overlying Lower Triassic (Induan) Kangshare Formation consists of thin-bedded, bioclastic packstone/wackestone that has a conformable contact with the underlying strata; the PTB is defined by the first occurrence of the conodont Hindeodus parvus and the

Griesbachian/Dienerian substage boundary is recognized by the first occurrence of the ammonoid Gyronites dubius (Fig. 3) based on the Dienerian ammonoid biostratigraphy framework proposed by Ware et al., (2015).

The Gongpu section is situated ~1 km west of Gongpu village, ~21 km south of the capital of Gyirong County. Detailed biostratigraphic work in this region was conducted by Garzanti (1998). The uppermost Permian Qubuerga Formation (Lopingian) can be subdivided into a lower, dark grey shale and an upper crinoid packstone that yields Lopingian-aged crinoids and brachiopods (Garzanti et al., 1998). The Lower Triassic Kangshare Formation is homogenous, and comprised of massive dolostone that contains conodont zones that range from the Dienerian to the Spathian (Garzanti et al., 1998); overlying massive fossiliferous limestone contains the Middle Triassic (Anisian) ammonoid Japonites sp. (Fig. 3).

The Tulong section is situated ~1 km west of Tulong village, 36 km NW of the capital of Nyalam County. The uppermost Permian Qubuerga Formation (Lopingian) consists of massive, dark grey shale containing few fossils except for some unidentifiable brachiopods and arthropods (Shen et al., 2006; Brühwiler et al., 2009); this unit strikingly resembles the Upper Permian Kuling Shales of Spiti (Northern India). The overlying thin-bedded dolostones of the lowermost Triassic (Induan) Kangshare Formation contain abundant conodonts including Hindeodus parvus, Clarkina carinata, and Cl. planate, and the ammonoids Ophiceras and Gyronites, indicating a Griesbachian to Dienerian age (Shen et al., 2006; Brühwiler et al., 2009). The thin-bedded dolostone is overlain by massive dark shale; the Griesbachian/Dienerian substage boundary is defined by the occurrence of the conodont Sweetospathodus kummeli and the ammonoid Gyronites (Brühwiler et al., 2009).

The Qubu section is located about 60 km east of the Tulong section. Similar to the Tulong section, the uppermost Permian (Lopingian) Qubuerga Formation consists of massive, dark grey shale, which is conformably overlain by thin-bedded dolostone of the lowermost Triassic Kangshare Formation (Fig. 2). The Qubuerga Formation yields brachiopods including Biplatyconcha grandis, Fusispirifer semiplicatis and Megasteges nepalensis, which suggest a Late Permian age (Shen et al., 2003). The thin-bedded dolostones of the Kangshare Formation contains a few conodonts, including Hindeodus parvus, and Clarkina carinata, as well as the ammonoids Ophiceras and Otoceras (Shen et al., 2006; Zhang et al., 2017), which indicate a Griesbachian age. The first and the only occurrence of the conodont Hindeodus parvus is 60 cm above the base of the thin-bedded orange dolostone, which was defined as the PTB by Shen et al. (2006). The PTB is interpreted to be the lithologic contact between the uppermost Permian shale and the overlying lowermost Triassic dolostone based on lithofacies, biofacies, and sequence stratigraphic correlations among the South Tibet sections. Therefore, the PTB at the Qubu section is placed at the base of Kangshare Formation (Fig. 2). The Griesbachian/Dienerian substage boundary is recognized by the appearance of the ammonoid Gyronites dubius (Fig. 3).

RESULTS

Facies descriptions, associations and interpretations

The uppermost Permian and Lower Triassic in South Tibet is highly condensed (Fig. 2) and characterized by a lack of macro-sedimentary fabrics (Garzanti et al., 1998; Shen et al., 2006; Brühwiler et al., 2009). Therefore, detailed microfacies analysis, based on high-resolution sampling was carried out around the PTB. The sample position of thin sections are prefixed with a – sign or a + sign depending on the distance below or above the Permian-Triassic boundary that the sample was removed from.

In South Tibet, the Upper Permian Selong Group consists of four microfacies, while the Lower Triassic Kangshare Formation consist of eight (Table 1); microfacies are classified based on lithology, bioclastic composition, and texture. Textural and facies definitions follow the classification scheme of Dunham (1962). Microfacies were identified and subdivided into three associations representing ramp sub-environments, including inner ramp, middle ramp, and outer ramp. Detailed features of microfacies and their corresponding sedimentary environment are summarized in Table 1.

Microfacies association 1: Bioclastic grainstone-dominated inner ramp

Description: The inner ramp association includes microfacies MF1, MF2 and MF3.

Calcrete (MF1) displays a crust-like structure comprised of multiple generations of laminae that grew in a downwards direction (Fig. 4A); these micro-laminae are characterized by irregular boundaries, are discontinuous laterally, and exhibit some brown pigmentation. Crinoid grainstone (MF2) predominantly consists of crinoid fragments (Fig. 4B) and shows cross stratification. Coral-bearing grainstone (MF3) is typified by the occurrence of rugose coral floating in crinoid grainstone. The corals are slightly abraded and infiltrated with the surrounding matrix (Fig. 4C). This microfacies association occurs in the uppermost horizons of the Selong Group at Selong, which is comprised of thick-bedded crinoid grainstone (MF2), overlain by a medium-bedded coral-bearing grainstone (MF3), and is topped by a thin layer of calcrete (MF1).

Interpretations: The inner ramp microfacies association is characterized by high energy deposits that formed above fair-weather wave base, frequent shifts in microfacies and occasional subaerial exposure (Burchette & Wright, 1992; Flügel, 2010). The thick-bedded, cross stratified crinoid grainstone is interpreted to record a high energy, shallow shoal (Hips, 1998; Shen et al., 2003a). The development of a very thin layer (several centimeters) of calcrete at the top of the coral bearing-bed implies transient subaerial exposure of the carbonate platform (Shen et al., 2006).

Microfacies association 2: Tempestite-dominated middle ramp

Description: The middle ramp association consists of microfacies MF4, MF5 and MF6, and is restricted to the Lower Triassic Kangshare Formation at the Selong section. The bivalve grainstone (MF4) is characterized by densely packed shells, in association with well-rounded micritic intraclasts (Fig. 4D); MF4 is commonly intercalated with bioclastic packstone (MF5) that consists of a relatively high diversity of fossils including foraminifera, echinoderms, bivalves, ostracods, and gastropods (Fig. 4E). Compared to MF5, bioclastic wackestone/floatstone (MF6) (Fig. 4F) contains less abundant fossils, which include bivalves, foraminifera, and echinoderms, and shows a matrix-supported texture.

Interpretation: The middle carbonate ramp zone is located between fair-weather wave base and storm wave base (Hips, 1998; Bádenas & Aurell, 2001). Micro-sedimentary textures indicative of strong bottom currents, likely induced by storm events are common, e.g., dense packing of bivalves and the associated with well-rounded intraclasts (MF4) (Pérez-López & Pérez-Valera, 2012). Bioclastic packstone/wackestone with diverse fossils (MF6), including pelagic ammonoids, are interpreted to represent lower energy conditions towards the deeper, distal middle ramp.

Microfacies association 3: Rudstone-dominated outer ramp

Description: The outer ramp association comprises six microfacies (MF7-MF12). Bryozoan-echinoderm rudstone (MF7) only occurs in the Upper Permian Selong Group at the Selong section and is characterized by highly abraded, brecciated bioclasts, including bryozoans, crinoids, and brachiopods with abundant micro-borings (Figs. 5A, B). Heavily abraded crinoid packstone/wackestone (MF8) (Fig. 5C) only occurs in the uppermost

Permian Qubuerga Formation at the Gongpu section. Dolomitic bioclastic wackestone/mudstone (MF9) (Fig. 5D), containing sparse echinoderms, thin-shelled bivalves, calcispheres, and ostracods, is widespread in the lowermost Kangshare Formation. Deep-water carbonate microfacies (thin-shelled bivalve packstone/wackestone (MF10) (Fig. 5E), pure lime-mudstone (MF11) and ammonoid-calcisphere wackestone (MF12) (Fig. 5F)), are common in the Lower Triassic Kangshare Formation at the Tulong and Qubu sections.

Interpretation: The outer ramp association was below the influence of storm events (Burchette & Wright, 1992; Ahr, 1998). Thin-bedded bryozoan-echinoderm rudstone (MF7) with micro-breccia fabric intercalated with massive dark-grey shale (Fig. 6), suggests a distal outer ramp environment (e.g. Kietzmann et al., 2014). The heavily abraded crinoid packstone/wackestone with rare bryozoan fragments seen at Gongpu are likely to have been transported into a distal, outer ramp setting (Garzanti et al., 1998). Abundant deep-water thin-shelled bivalves, pelagic calcispheres (interpreted as calcified (?) radiolarians, Brühwiler et al., 2009), and ammonoids indicate a deep outer ramp setting (e.g. Lukeneder et al., 2012), which is supported by the absence of micro- and macro-sedimentary textures indicative of strong bottom currents.

Evolution of depositional settings across the PTB

Selong section

The vertical distribution of the uppermost Permian microfacies association at the Selong section reveals a sudden environmental transition from lower outer ramp to upper inner ramp 1.0 m beneath the PTB (Fig. 6). The lower outer ramp association predominantly consists of thin-bedded bryozoan rudstone (MF7) that exhibits breccia fabrics (Figs. 7B, C), and is intercalated with massive dark-grey shale, suggesting an outer ramp environment (e.g. Kietzmann et al., 2014). The inner ramp association is composed of, in ascending order, cross-bedded crinoid grainstone (MF2) (Fig. 7D), thin-bedded coral-bearing grainstone (MF3) (Fig. 7E) and a very thin layer of calcrete (MF1), revealing the transition from a high energy shallow shoal to transient subaerial exposure. The overlying PTB occurs in a thin-bedded orange dolostone (Fig. 7A).

Examination of the lowermost Triassic microfacies association at the Selong section shows the inner ramp was abruptly succeeded by a middle ramp setting (Fig. 6). The inner ramp association is comprised of thin-bedded, crinoid grainstone/packstone, which is sharply overlain by intercalations of thin-bedded tempestites (MF4) and bioclastic wackestone consistent with low energy, middle ramp deposits (MF5, MF6). The middle ramp association is capped by a thin interval of thin-shelled bivalve wackestone (MF10), which corresponds to an outer ramp environment.

Gongpu section

The uppermost Permian microfacies association at the Gongpu section is characterized by a sudden upward transition from massive, dark grey shale to thick-bedded, heavily abraded, crinoid packstone/wackestone (MF8) (Figs. 8 and 9A) that lacks any structures and/or textures that are indicative of shallow, high energy environments (i.e. cross-bedding, wave ripples, and a well-sorted texture). The highly abraded crinoid fragments, in association with bryozoan fragments floating in a dolomicrite matrix (Fig. 9B), suggests that the bioclastic fragments were allochthonous, and were transported and deposited in a deep, outer ramp environment.

The Lower Triassic microfacies association shows a monotonous succession of dolomitic bioclastic wackestone/mudstone (MF9) (Fig. 9C), corresponding to a stable, deep ramp environment. The Lower Triassic dolomitic bioclastic wackestone is overlain by an uppermost Lower Triassic bioclastic packstone with diverse fossils (MF5) (Fig. 9D) including the foraminifera Dentalina sp. (Fig. 9E).

Tulong section

The uppermost Permian Qubuerga Formation is characterized by a sudden transition from a lower, ~10m-thick, dark grey shale to a thin-bedded, greenish-grey silty shale (Fig. 10) formed in a stable, distal ramp environment. The contact between the greenish shale and the overlying thick-bedded dolostone marks the PTB (Brühwiler et al., 2009) (Fig. 11A).

The overlying lowermost Triassic Kangshare Formation consists of thick-bedded dolomitic bioclastic wackestone/mudstone (MF9) (Figs. 11B to 11D) and contains occasional echinoderms, thin-shelled bivalves, and ammonoids, which suggest a deep water, distal ramp environment. The Griesbachian-Dienerian boundary is marked by the occurrence of a thin-bedded thin-shelled, bivalve packstone/wackestone (Fig. 11E), which is embedded in massive dark grey shale. The dolomitic bioclastic wackestone/mudstone (MF9) is overlain by massive dark grey shale that is Dienerian in age (Fig. 10).

Qubu section

The lithology of the latest Permian Qubuerga Formation at Qubu is comparable with that at Tulong across the same stratigraphic interval, which is characterized by a sudden transition from a lower dark grey shale to an overlying thin-bedded greenish, silty shale (Figs. 12 and 13A), indicating a persistent distal ramp environment.

The microfacies association of the lowermost Triassic Kangshare Formation at Qubu also shows a striking similarity to the one from the Tulong section, which is predominantly comprised of dolomitic bioclastic wackestone/mudstone (MF9) (Figs. 13B to 13D). Occasional echinoderm fragments, the small foraminifera Nodosaria sp. and Glomospira sp. (Figs. 13C, D), and thin-shelled bivalves, as well as ammonoids occur within the dolomitic wackestone. A thin-bedded ammonoid-calcisphere wackestone (Fig. 13E) occurs at the base of the Dienerian, and is intercalated with bioclastic wackestone that contains occasional thin-shelled bivalves and ostracods.

DISCUSSION

Evolution of the carbonate factory across the PTB

Carbonate factories can be subdivided into cool-water (dominated by the Heterozoan Association) and warm-water types (dominated by the Chlorozoan Association) based on their carbonate producing faunas (Carannante et al., 1988; James et al., 1997; Schlager, 2003). South Tibet witnessed a sudden transition from a cool-water, heterozoan dominated carbonate factory to a benthic automicrite factory with only thin-shelled bivalves contributing significant carbonate to the sediment.

A Late Permian cool-water carbonate factory is recognized based on the type of carbonate producing faunas and microfacies analysis (Fig. 14). The source of lime mud during the Late Permian in South Tibet is a cool-water metazoan community that includes bryozoans, echinoderms and brachiopods. Bryozoan grainstones from the middle Late Permian Selong group (22.4 m below PTB) consist of in situ bryozoans, implying that the bryozoan-dominated community weakly trapped grains within the lime mud. Large mounds/reefs are absent in South Tibet; instead, bryozoans, echinoderms, and cool-water brachiopods are concentrated in thin-bedded limestones intercalated with massive dark grey shales. Evidence for a cool-water carbonate factory is also supported by the occurrence of weak, early diagenetic cements, resulting in well preserved micro-borings that are infilled with micrite in bioclasts (Figs. 5A, B). This latest Permian carbonate factory shows some similarity to those from carbonate ramps dominated by upwelling that developed in the transitional zone between the cool-water and warm-water realms (James et al., 1997).

The Early Triassic carbonate platform of South Tibet consists mainly of homogenous dolomudstone that contains lesser amounts of bioclasts, including bivalves, echinoderms, ostracods and small foraminifera. The four Lower Triassic sections from South Tibet are highly condensed (Garzanti et al., 1998; Brühwiler et al., 2009) and carbonate sedimentation rates are low, with an average value of ~ 6.5 m $m.a.^{-1}$, indicating dampened carbonate production within the Early Triassic "biogenic" carbonate factory. The consistent lithofacies throughout the four sections in South Tibet, in combination with the lack of slide, slump, and debris flows, suggests the widespread development of a low gradient, homoclinal ramp (Fig. 15).

Controls on the evolution of the carbonate ramp across the PTME

Geotectonic setting

South Tibet and the northern Lhasa Block were once located on the northern margin of peri-Gondwana. At the end of the Paleozoic, the Lhasa Block began to drift northward, leading to the opening of the Neo-Tethys and the development of a widespread passive margin (Liu & Einsele, 1994). Lower Triassic strata from Spiti, India (Bhargava et al., 2004), Manang, Nepal (Garzanti et al., 1994; Yoshida et al., 2014) and South Tibet (Brühwiler et al., 2009; Shen et al., 2003a) demonstrate a high degree of correlation with regards to lithology, biostratigraphy and sequence stratigraphy, indicating uniform subsidence rates across the passive margin. Subsidence rates during the Early Triassic are estimated to have been slow (~18 m $m.a.^{-1}$) (Liu & Einsele, 1994); the low, uniform subsidence rates of passive continental margins favour the formation of homoclinal carbonate ramps (Chatalov, 2013, 2016). This is because passive continental margins provide a flat base for carbonate accumulation and hinders detrital input (Chatalov, 2016). Sections from South Tibet contain low amounts of detrital grains, including quartz, mica and feldspar, indicating a low detritus input from the landmass. A gradual transgression along the passive margin during the Early Triassic (discussed below) accelerated drowning of the carbonate platform, which resulted in the widespread development of dark grey shale during the uppermost Induan (Fig. 2).

The end-Permian regression and the following Early Triassic transgression

Analysis of uppermost Permian microfacies associations from South Tibet reveals a rapid regression. This rapid regression has been reported widely, including along the northern margin of peri-Gondwana (Wignall & Hallam, 1993; Baud et al., 1996), in the Western Tethys (Tavakoli et al., 2017) and in the Eastern Tethys (Yin et al., 2014). This rapid global regression is clearly reflected in the Selong section by the sudden shift from a lower outer ramp microfacies association to an inner ramp microfacies association, along with transient subaerial exposure. Other Late Permian sections that were deposited in deep shelf environments, i.e., Tulong (South Tibet), Spiti (India) (Ghosh et al., 2016), Manang (Nepal) (Garzanti et al., 1994), also show evidence of a rapid regression at the end of Permian..

Study of lowermost Triassic microfacies from South Tibet indicates a rapid transgression immediately following the latest Permian regression (Fig. 16). This transgression has been reported widely from the northern margin of peri-Gondwana (Wignall & Hallam, 1993; Baud et al., 1996) and the Eastern Tethys (Wignall & Hallam, 1993; Yin et al., 2014). This global transgression is recorded at the Selong section by the rapid transition from caliche (calcrete) at the PTB to lowermost Triassic thin-bedded crinoid packstone/wackestone, which is overlain by a shelly tempestite. The earliest Triassic transgression is manifested at the other South Tibet sections by a transition from lowermost Triassic thin-bedded dolomitic bioclastic wackestone/mudstone to overlying dark grey shale.

Carbonate-producing faunas

The PTME is the largest biotic crisis of the Phanerozoic, and lead to the loss of many heavily calcified metazoans including numerous corals, brachiopods, bryozoans, and calcareous algae (Erwin, 1994; Chen and Benton, 2012), and resulted in a global change in the nature of carbonate factory production in both subtropical to tropical regions and high latitude regions (Kiessling et al., 2003; Pomar & Hallock, 2008).

The loss of reefs from subtropical and tropical regions resulted in the development of widespread microbialites in shallow open shelves and ramps (Hips, 1998; Xie et al., 2010; Vennin et al., 2015), a change attributed to the unusual chemistry of Early Triassic oceans

(Woods et al., 2007; Kershaw et al., 2011) and/or a bloom of bacteria that was the result of depressed grazing pressures by metazoans due to the mass extinction (Schubert & Bottjer, 1992; Xie et al., 2010).

The pattern of carbonate factory evolution in South Tibet across the PTME is different to that in the subtropical to tropical regions. Microbialites are noticeably absent, instead, the PTB carbonate platform from South Tibet is dominated by homogenous dolomitic lime mudstone/wackestone with rare mollusks and echinoderms bioclasts (Fig. 16). The absence of microbialites is likely because of either the high palaeolatitude of South Tibet that resulted in relatively low sea surface temperatures and/or the deep-water depths of the South Tibet sections, which did not allow the growth of microbialites.

The source of lime mud in South Tibet was likely from the metabolic activities of heterotrophic bacteria. The Early Triassic ocean is characterized by a high nutrient influx (Algeo and Twitchett, 2010), blooms of cyanobacteria (Xie et al., 2005, 2010) and widespread ocean anoxia (Wignall and Twitchett, 2002); these conditions would favour heterotrophic bacteria in deep waters, especially sulfate-reducing bacteria. The elevated alkalinity of seawater caused by sulfate reduction, coupled with elevated surface ocean temperatures (discussed below), would significantly promote the rapid precipitation of dolomicrite (Kempe and Kazmierczak, 1994; Bergmann et al., 2013). A global PTB dolostone "event" has been reported and linked to intense microbial sulfate reduction (Li et al., 2018b), indicating that the benthic-automicrite carbonate factory plays a significant role in carbonate production during the Early Triassic.

Climate conditions

Cool waters persisted in South Tibet during the Late Permian, as inferred by the presence of typical Late Permian cold-water brachiopods, including Taeniothaerus, and Trigonotreta, and the large, thick-shelled Spiriferella, and Neospirifer (Shen et al., 2006), and an overall cool-water assemblage (Bryonoderm) (Fig. 16). The Bryonoderm carbonate-producing assemblage is characterized by low carbonate production rates (Schlager, 2003), and was prevalent in temperate to cool areas during the Late Permian (Beauchamp, 1997; Ehrenberg et al., 2001; Kiessling et al., 2003).

Global warming took place at the end of Permian due to the outgassing of huge amounts of CO_2 from Siberian Trap volcanism (e.g. Joachimski et al., 2012; Sun et al., 2012; Song et al., 2019); it is estimated that the average sea surface temperature increased from 20˚C to 32˚C in the equatorial regions (Sun et al., 2012). Therefore, lethally hot sea surface temperatures have been proposed as one of the potential mechanisms for the PTME. Although South Tibet was situated in the southern mesothermal temperate zone (Shen et al., 2006), it was also affected by warming. The end-Permian warming event in South Tibet is reflected by a faunal change from a cool-water community to warm-water community. The intrusion of warm-water species such as the conodont Clarkina spp., and the brachiopod Tethyochonetes at the Selong section (Shen et al., 2006) provide evidence of warming sea surface temperatures at the PTB.

The transition from a cool-water carbonate factory to a warm-water carbonate factory is often associated with increased carbonate production (Carannante et al., 1988; James et al., 1997; Schlager, 2000, 2003), but this is not the case for South Tibet at the PTB. Instead, the loss of diversity within groups such as bryozoans and echinoderms saw the development of a homoclinal carbonate ramp, which was characterized by low carbonate production rates.

CONCLUSIONS

Detailed microfacies analysis, combined with petrological study, reveals a dramatic shift in the deep water carbonate factory in response to the Permian-Triassic biotic crisis in South Tibet. A cool-water bryozoan-echinoderm dominated carbonate ramp developed in South Tibet during the Late Permian. The loss of most carbonate-producing faunas during the PTME, including bryozoans, brachiopods and echinoderms, led to the collapse of the Late Permian carbonate factory. Immediately following the PTME, a benthic automicrite factory with only minor amounts of calcifying metazoans developed, and consequently, a dolomite-dominated homoclinal carbonate ramp was widely present on the northern margin of peri-Gondwana. The carbonate factory transition as well as the development of the homoclinal ramp resulted from the combination of the following factors: (1) The loss of cool-water, calcifying metazoans due to Early Triassic global warming, allowing lime mud to be transported and redeposited uniformly across the carbonate ramp; (2) A slow and uniform subsidence rate, coupled with the Early Triassic transgression, allowed the maintenance of the flat morphology of the carbonate ramp along the northern margin of peri-Gondwana .

ACKNOWLEDGEMENTS

We thank Sedimentology editor Dr. Peir Pufahl, associate editor Catherine Reid, and reviewers Patrick Meister and Matthew Clapham for their constructive comments on this paper. We thank Shouyi Jiang and Fengyu Wang for field work assistance, Xiaokang Liu for foraminifera identification. We are also grateful for the help from the Forestry Bureau, Department of Land and Resources and Everest Protection Agency in Tibet, China. This study is supported by the National Natural Science Foundation of China (41821001, 41622207, 41530104, 41661134047), and the 111 Project (B08030). This study is a contribution to the IGCP 630.

REFERENCES

Ahr, W.M. (1998) Carbonate ramps, 1973-1996: a historical review. Geol. Soc. London Spec. Publ., **149**, 7–14.

Algeo, T.J. and **Twitchett, R.J.** (2010) Anomalous Early Triassic sediment fluxes due to elevated weathering rates and their biological consequences. Geology, **38**, 1023–1026.

Bádenas, B. and **Aurell, M.** (2001) Proximal–distal facies relationships and sedimentary processes in a storm dominated carbonate ramp (Kimmeridgian, northwest of the

Iberian Ranges, Spain). Sediment. Geol., **139**, 319–340.

Baud, A., Atudorei, V. and **Sharp, Z.** (1996) Late Permian and Early Triassic evolution of the Northern Indian margin: Carbon isotope and sequence stratigraphy. Geodin. Acta, **9**, 57–77.

Baud, A., Richoz, S. and **Pruss, S.** (2007) The Lower Triassic anachronistic carbonate facies in space and time. Glob. Planet. Change, **55**, 81–89.

Beauchamp, B. (1997) Permian warm- to very cold-water carbonates and cherts in northwest Pangea. Spec. Publ. Sepm, 327–347.

Bergmann, K.D., Grotzinger, J.P. and **Fischer, W.W.** (2013) Biological influences on seafloor carbonate precipitation. Palaios, **28**, 99–115.

Bhargava, O.N., Krystyn, L., Balini, M., Lein, R. and **Nicora, A.** (2004) Revised litho-and sequence stratigraphy of the Spiti Triassic. Albertiana, **30**, 21–39.

Brühwiler, T., Goudemand, N., Galfetti, T., Bucher, H., Baud, A., Ware, D., Hermann, E., Hochuli, P.A. and **Martini, R.** (2009) The Lower Triassic sedimentary and carbon isotope records from Tulong (South Tibet) and their significance for Tethyan palaeoceanography. Sediment. Geol., **222**, 314–332.

Burchette, T.P. and **Wright, V.P.** (1992) Carbonate ramp depositional systems. Sediment. Geol., **79**, 3–57.

Carannante, G., Esteban, M., Milliman, J.D. and **Simone, L.** (1988). Carbonate lithofacies as paleolatitude indicators: Problems and limitations. Sediment. Geol., **60**, 333–346.

Chatalov, A. (2013) A Triassic homoclinal ramp from the Western Tethyan realm, Western Balkanides, Bulgaria : Integrated insight with special emphasis on the Anisian outer to inner ramp facies transition. Palaeogeogr. Palaeoclimatol. Palaeoecol., **386**, 34–58.

Chatalov, A. (2016) Global, regional and local controls on the development of a Triassic carbonate ramp system, Western Balkanides, Bulgaria. Geol. Mag., 1–33.

Chen, Z.Q. and **Benton, M.J.** (2012) The timing and pattern of biotic recovery following the end-Permian mass extinction. Nat. Geosci., **5**, 375–383.

Cozzi, A., Grotzinger, J.P. and **Allen, P.A.** (2004) Evolution of a terminal Neoproterozoic carbonate ramp system (Buah Formation, Sultanate of Oman): Effects of basement paleotopography. Geol. Soc. Am. Bull., **116**, 1367–1384.

Dunham, R.J. (1962) Classification of carbonate rocks according to depositional texture. Aapg Mem., **1**, 108–121.

Ehrenberg, S.N., Pickard, N.A.H., Henriksen, T.A., Svana, Gutteridge, P. and **Macdonald, D.** (2001) A depositional and sequence stratigraphic model for cold-water, spiculitic strata based on the Kapp Starostin Formation (Permian) of Spitsbergen and equivalent deposits from the Barents Sea. Am. Assoc. Pet. Geol. Bull., **85**, 2061–2087.

Erwin, D.H. (1994) The Permo-Triassic extinction. Nature, **367**, 231–236.

Flügel, E. (2010) Microfacies of Carbonate Rocks. Springer, Berlin Heidelberg, p. 1-929.

Garzanti, E., Nicora, A. and **Tintori, A.** (1994) Triassic stratigraphy and sedimentary evolution of the Annapurna Tethys Himalaya (Manang area, Central Nepal). Riv. Ital. Paleontol. Stratigr., **100**, 195–226.

Garzanti, E., Nicora, A. and **Rettori, R.** (1998) Permo-Triassic boundary and Lower to Middle Triassic in South Tibet. J. Asian Earth Sci., **16**, 143–157.

Ghosh, N., Basu, A.R., Bhargava, O.N., Shukla, U.K., Ghatak, A., Garzione, C.N. and **Ahluwalia, A.D.** (2016) Catastrophic environmental transition at the Permian-Triassic Neo-Tethyan margin of Gondwanaland: Geochemical, isotopic and sedimentological evidence in the Spiti Valley, India. Gondwana Res., **34**, 324–345.

Grotzinger, J.P., Knoll, A.H. (1995) Anomalous carbonate precipitates: Is the Precambrian the key to the Permian? Palaios, **10**, 578–596.

Grotzinger, J.P. and **Knoll, A.H.** (1999) Stromatolites in Precambrian carbonates: Evolutionary mileposts or environmental dipsticks? Annu. Rev. Earth Planet. Sci., **27**, 313–358.

Heindel, K., Richoz, S., Birgel, D., Brandner, R., Klügel, A., Krystyn, L., Baud, A., Horacek, M., Mohtat, T. and **Peckmann, J.** (2015) Biogeochemical formation of calyx-shaped carbonate crystal fans in the subsurface of the Early Triassic seafloor. Gondwana Res., **27**, 840–861.

Hermann, E., Hochuli, P.A., Bucher, H. and **Roohi, G.** (2012) Uppermost Permian to Middle Triassic palynology of the Salt Range and Surghar Range, Pakistan. Rev. Palaeobot. Palynol., **169**, 61–95.

Hips, K. (1998) Lower Triassic storm-dominated ramp sequence in northern Hungary: An example of evolution from homoclinal through distally steepened ramp to Middle Triassic flat-topped platform. Carbonate Ramps, **149**, 315–338.

James, N.P., Bone, Y., Hageman, S., Gostin, V.A. and **Andfeary, D.A.** (1997) Cool-water carbonate sedimentation during the Terminal Quaternary, high-amplitude, sea-level cycle: Lincoln Shelf, Southern Australia. In: Cool-Water Carbonates James (Eds N.P., James and J.A.D. Clarke), SEPM. Spec. Publ., **56**, p. 53–76.

Joachimski, M.M., Lai, X., Shen, S., Jiang, H., Luo, G., Chen, B., Chen, J. and **Sun, Y.** (2012) Climate warming in the latest Permian and the Permian-Triassic mass extinction. Geology, **40**, 195–198.

Kempe, S. and **Kazmierczak, J.** (1994) The role of alkalinity in the evolution of ocean chemistry, organization of living systems, and biocalcification processes. Prep. Biochem., **7**, 345–355.

Kershaw, S., Zhang, T. and **Lan, G.** (1999) A ?microbialite carbonate crust at the Permian-Triassic boundary in South China, and its palaeoenvironmental significance. Palaeogeogr. Palaeoclimatol. Palaeoecol., **146**, 1–18.

Kershaw, S., Crasquin, S., Forel, M.B., Randon, C., Collin, P.Y., Kosun, E., Richoz, S.

and **Baud, A.** (2011) Earliest Triassic microbialites in Çürük Dag, southern Turkey: Composition, sequences and controls on formation. Sedimentology, **58**, 739–755.

Kiessling, W., Flügel, E. and **Golonka, J.** (2003) Patterns of Phanerozoic carbonate platform sedimentation. Lethaia, **36**, 195–225.

Kietzmann, D.A., Palma, R.M., Riccardi, A.C., Martín-Chivelet, J. and **López-Gómez, J.** (2014) Sedimentology and sequence stratigraphy of a Tithonian–Valanginian carbonate ramp (Vaca Muerta Formation): A misunderstood exceptional source rock in the Southern Mendoza area of the Neuquén Basin, Argentina. Sediment. Geol., **302**, 64–86.

Lehrmann, D.J. (1999) Early Triassic calcimicrobial mounds and biostromes of the Nanpanjiang basin, south China. Geology, **27**, 359–362.

Li, M., Song, H.J, Tian, L., Woods, A.D., Dai, X. and **Song, H.Y** (2018a) Lower Triassic deep sea carbonate precipitates from South Tibet, China. Sediment. Geol., **376**, 60–71.

Li, M., Song, H.J, Algeo, T.J., Wignall, P.B., Dai, X. and **Woods, A.D.** (2018b) A dolomitization event at the oceanic chemocline during the Permian-Triassic transition. Geology, **46**, 1043–1046.

Liu, G. and **Einsele, G.** (1994) Sedimentary history of the Tethyan basin in the Tibetan Himalayas. Geol. Rundschau, **83**, 32–61.

Lukeneder, S., Harzhauser, M., İslamoğlu, Y., Krystyn, L. and **Lein, R.** (2012) A delayed carbonate factory breakdown during the Tethyan-wide Carnian Pluvial Episode along the Cimmerian terranes (Taurus, Turkey). Facies, **58**, 279–296.

Orchard, M., Nassichuk, W. and **Rui, L.** (1994) Conodonts from the Lower Griesbachian Otoceras latilobatum bed of Selong, Tibet and the position of the P-T boundary. Cspg Spec. Publ., **17**, 823–843.

Pérez-López, A. and **Pérez-Valera, F.** (2012) Tempestite facies models for the epicontinental Triassic carbonates of the Betic Cordillera (southern Spain). Sedimentology, **59**, 646–678.

Pomar, L. and **Hallock, P.** (2008) Carbonate factories: A conundrum in sedimentary geology. Earth-Sci. Rev., **87**, 134–169.

Pruss, S.B., Corsetti, F.A. and **Fischer, W.W.** (2008) Seafloor-precipitated carbonate fans in the Neoproterozoic Rainstorm Member, Johnnie Formation, Death Valley Region, USA. Sediment. Geol., **207**, 34–40.

Raup, D.M. and **Sepkoski, J.J.** (1982) Mass extinctions in the marine fossil record. Science, **215**, 1501.

Schlager, W. (2000) Sedimentation rates and growth potential of tropical, cool-water and mud-mound carbonate systems. Geol. Soc. London Spec. Publ., **178**, 217–227.

Schlager, W. (2003) Benthic carbonate factories of the Phanerozoic. Int. J. Earth Sci., **92**, 445–464.

Schubert, J.K. and **Bottjer, D.J.** (1992) Early Triassic stromatolites as post-mass extinction disaster forms. Geology, **20**, 883–886.

Sepkoski, Jr, J.J., **Bambach, R.K.** and **Droser, M.L.** (1991) Secular changes in Phanerozoic event bedding and the biological overprint. In: Cycles and Events inStratigraphy (Ed. by G. Einsele, W. Ricken and A.Seilacher), Springer-Verlag, Berlin, p. 298–312.

Shen, S.Z., Archbold, N.W., Shi, G.R. and **Chen, Z.Q.** (2000) Permian brachiopods from the SelongXishan section, Xizang (Tibet), China Part 1: Stratigraphy, Strophomenida, Productida and Rhynchonellida. Geobios, **33**, 725–752.

Shen, S.Z., Shi, G.R. and **Archbold, N.W.** (2003) Lopingian (Late Permian) brachiopods from the Qubuerga Formation at the Qubu section in the Mt. Qomolangma region, southern Tibet (Xizang), China. Palaeontogr. Abt. A., **268**, 49–101.

Shen, S., Cao, C.Q., Shi, G.R., Wang, X.D. and **Mei, S.L.** (2003a) Lopingian (Late Permian) stratigraphy, sedimentation and palaeobiogeography in southern Tibet. Newsletters Stratigr., **39**, 157–179.

Shen, S., Sun, D. and **Shi, G.R.** (2003b) A biogeographically mixed late Guadalupian (late Middle Permian) brachiopod fauna from an exotic limestone block at Xiukang in Lhaze county, Tibet. J. Asian Earth Sci., **21**, 1125–1137.

Shen, S.Z., Cao, C.Q., Henderson, C.M., Wang, X.D., Shi, G.R., Wang, Y. and **Wang, W.** (2006) End-Permian mass extinction pattern in the northern peri-Gondwanan region. Palaeoworld, **15**, 3–30.

Song, H.J, Wignall, P.B., Tong, J.N, and **Yin, H.F.** (2013) Two pulses of extinction during the Permian–Triassic crisis. Nat. Geosci., **6**, 52–56.

Song, H.J, Wignall, P. B., Song, H.Y, Dai, X., and **Chu, D.L.** (2019) Seawater temperature and dissolved oxygen over the past 500 million years. J. Earth Sci., **30**: doi: 10.1007/s12583-12018-11002-12582.

Sun, Y.D., Joachimski, M.M., Wignall, P.B., Yan, C.B., Chen, Y.L., Jiang, H.S., Wang, L. and **Lai, X.L.** (2012) Lethally hot temperatures during the Early Triassic greenhouse. Science, **338**, 366–370.

Tavakoli, V., Naderi-Khujin, M. and **Seyedmehdi, Z.** (2017) The end-Permian regression in the western Tethys: Sedimentological and geochemical evidence from offshore the Persian Gulf, Iran. Geo-Marine Lett., **38**, 1–14.

Thomson, D., Rainbird, R.H. and **Dix, G.** (2014) Architecture of a Neoproterozoic intracratonic carbonate ramp succession: Wynniatt Formation, Amundsen Basin, Arctic Canada. Sediment. Geol., **299**, 119–138.

Vennin, E., Olivier, N., Brayard, A., Bour, I., Thomazo, C., Escarguel, G., Fara, E., Bylund, K.G., Jenks, J.F. and **Stephen, D.A.** (2015) Microbial deposits in the aftermath of the end-Permian mass extinction: A diverging case from the Mineral Mountains (Utah, USA). Sedimentology, **62**, 753–792.

Wang, L., Wignall, P.B., Sun, Y., Yan, C., Zhang, Z. and **Lai, X.** (2017) New Permian-Triassic conodont data from Selong (Tibet) and the youngest occurrence of Vjalovognathus. J. Asian Earth Sci., **146**, 152–167.

Ware, D., Bucher, H., Brayard, A., Schneebeli-Hermann, E. and **Brühwiler, T.** (2015) High-resolution biochronology and diversity dynamics of the Early Triassic ammonoid recovery: The Dienerian faunas of the Northern Indian Margin. Palaeogeogr. Palaeoclimatol. Palaeoecol., **440**, 363–373.

Wignall, P.B. and **Hallam, A.** (1993) Griesbachian (Earliest Triassic) palaeoenvironmental changes in the Salt Range, Pakistan and southeast China and their bearing on the Permo-Triassic mass extinction. Palaeogeogr. Palaeoclimatol. Palaeoecol., **102**, 215–237.

Wignall, P.B. and **Twitchett, R.J.** (2002) Extent, duration, and nature of the Permian-Triassic superanoxic event. Geol. Soc. Am. Spec. Pap., **356**, 395–413.

Wignall, P.B. and **Newton, R.** (2003) Contrasting deep-water records from the Upper Permian and Lower Triassic of South Tibet and British Columbia: Evidence for a diachronous mass extinction. Palaios, **18**, 153–167.

Woods, A.D., Bottjer, D.J., Mutti, M. and **Morrison, J.** (1999) Lower Triassic large sea-floor carbonate cements: Their origin and a mechanism for the prolonged biotic recovery from the end-Permian mass extinction. Geology, **27**, 645–648.

Woods, A.D., Bottjer, D.J. and **Corsetti, F.A.** (2007) Calcium carbonate seafloor precipitates from the outer shelf to slope facies of the Lower Triassic (Smithian-Spathian) Union Wash Formation, California, USA: Sedimentology and palaeobiologic significance. Palaeogeogr. Palaeoclimatol. Palaeoecol., **252**, 281–290.

Woods, A.D. (2009) Anatomy of an anachronistic carbonate platform: Lower Triassic carbonates of the southwestern United States. J. Geol. Soc. Aust., **56**, 825–839.

Woods, A.D. (2014) Assessing Early Triassic paleoceanographic conditions via unusual sedimentary fabrics and features. Earth-Sci. Rev., **137**, 6–18.

Xie, S., Pancost, R.D., Yin, H., Wang, H. and **Evershed, R.P.** (2005) Two episodes of microbial change coupled with Permo/Triassic faunal mass extinction. Nature, **434**, 494–497.

Xie, S., Pancost, R.D., Wang, Y., Yang, H., Wignall, P.B., Luo, G., Jia, C. and **Chen, L.** (2010) Cyanobacterial blooms tied to volcanism during the 5 m.y. Permo-Triassic biotic crisis. Geology, **38**, 447–450.

Yin, H., Jiang, H., Xia, W., Feng, Q., Zhang, N. and **Shen, J.** (2014) The end-Permian regression in South China and its implication on mass extinction. Earth-Sci. Rev., **137**, 19–33.

Yoshida, K., Kawamura, T., Suzuki, S., Deep, A., Ram, B., Shiga, Y., Adachi, Y. and **Raj, M.** (2014) Continental weathering in the Early Triassic in Himalayan Tethys, central Nepal: Implications for abrupt environmental change on the northern margin of Gondwanaland. J. Asian Earth Sci., **79**, 288–301.

Yuan, D.X., Zhang, Y.C. and **Shen, S.Z.** (2018) Conodont succession and reassessment of major events around the Permian-Triassic boundary at the Selong Xishan section, southern Tibet, China. Glob. Planet. Chang., **161**, 194–210.

Zhang, C., Bucher, H. and **Shen, S.Z.** (2017) Griesbachian and Dienerian (Early Triassic) ammonoids from Qubu in the Mt. Everest area, southern Tibet. Palaeoworld, **26**, 650–662.

Figure Caption

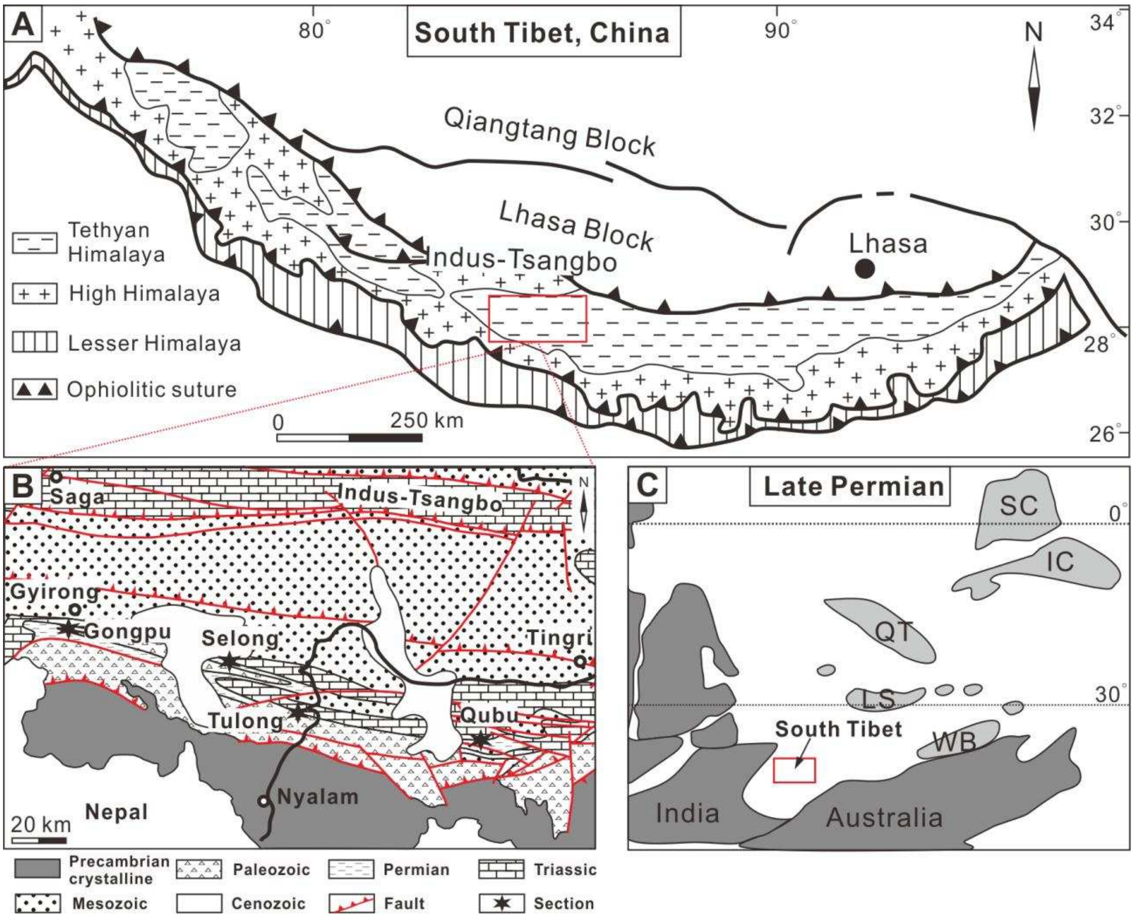

Fig. 1. (A) Geological map of the Himalaya region and study area (marked by the red rectangle), which is located within the middle Tethyan Himalaya region. Modified from Liu and Einsele (1994). (B) Geological and location map of the study sections (data is from the National Geological Archive, China). (C) Palaeogeographic map of Southern Tethys during the Late Permian (modified from Shen et al., 2003). South Tibet (red rectangle) was situated on the northern margin of the India Plate with a palaeolatitude of ~40˚S. 'WB', Western Burma; 'LS', Lhasa; 'QT', Qiangtang; 'IC', Indochina; 'SC', South China.

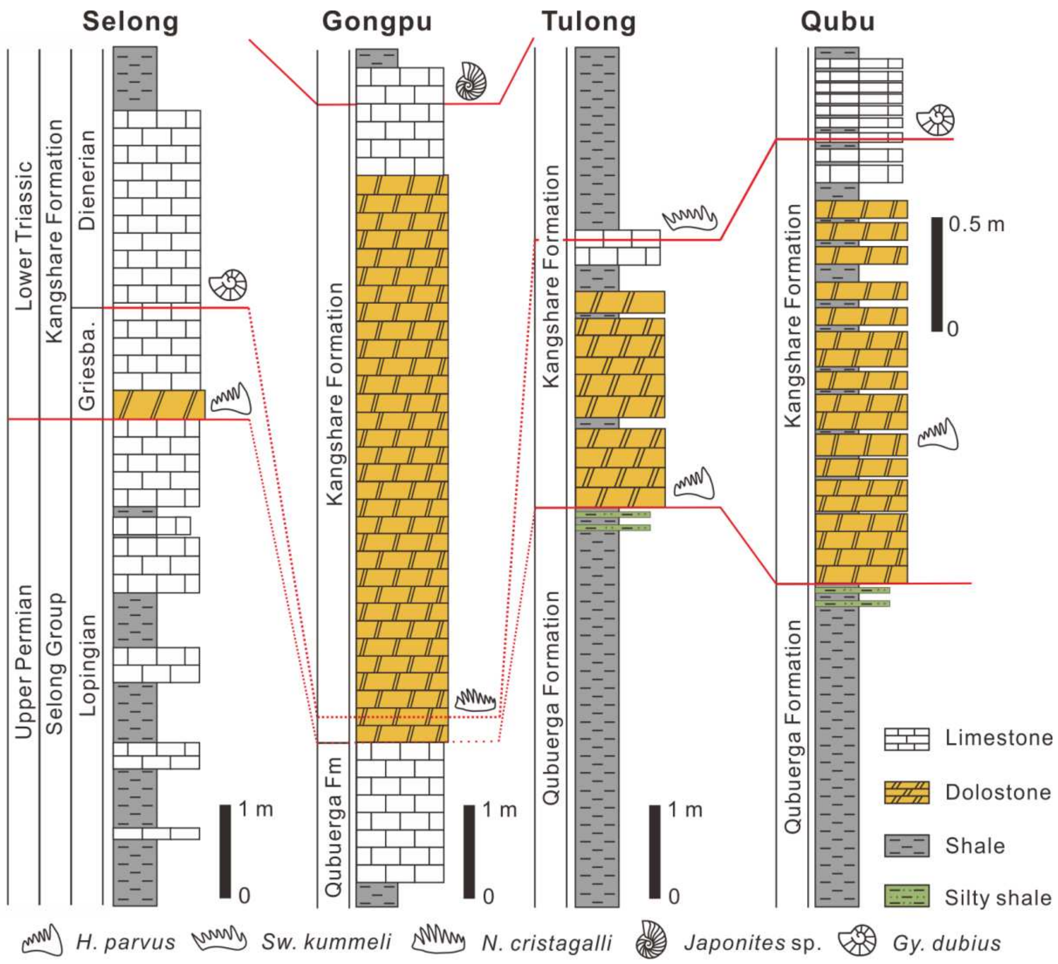

Fig. 2. Stratigraphic correlation and lithology of Permian-Triassic sections from the South Tibet region. The Permian-Triassic boundary (PTB) is recognized by the first occurrence of the conodont Hindeodus parvus (The PTB at Qubu section is slightly modified from Shen et al. (2006) based on lithofacies and sequence stratigraphy), the Griesbachian-Dienerian boundary is defined by the first occurrence of the conodont Sweetospathodus kummeli, Neospathodus cristagalli or the ammonoid Gyronites dubius and the Spathian-Anisian boundary is identified by the first occurrence of the ammonoid Japonites sp.. Conodont data from the Selong, Gongpu, Tulong and Qubu sections are from Garzanti et al. (1998), Shen et al. (2006), Brühwiler et al. (2009), and Wang et al. (2017). Red lines mark the

Permian-Triassic, Griesbachian-Dienerian, and Spathian-Anisian boundaries (solid line is determined and dashed line is undetermined).

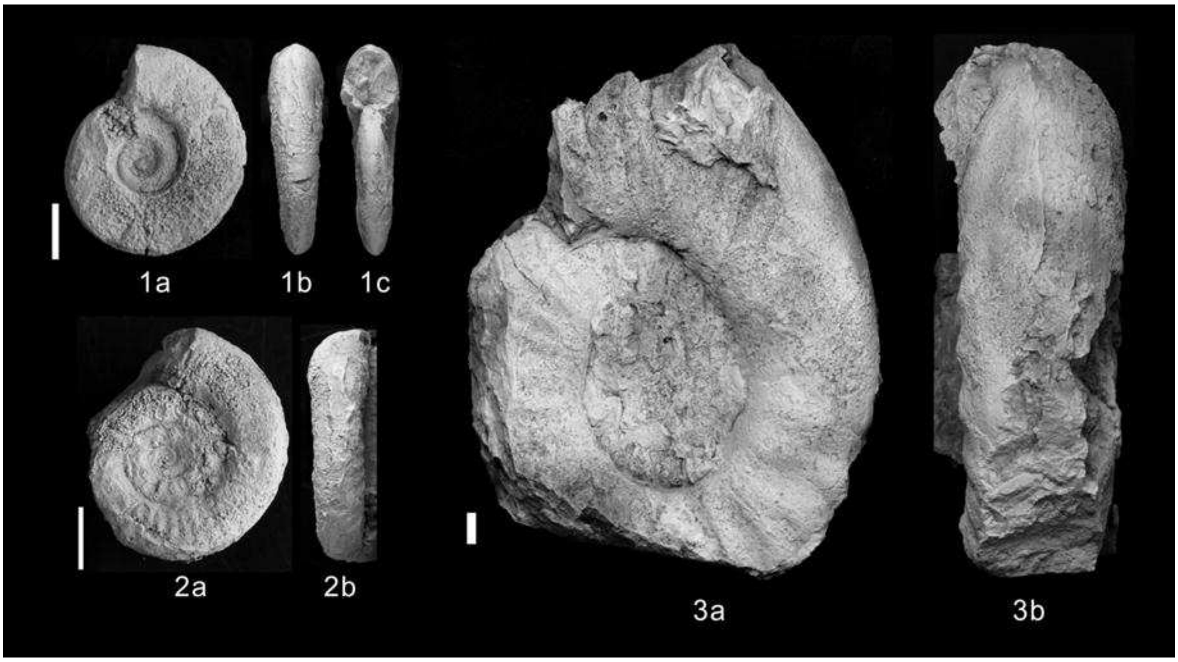

Fig. 3. Ammonoids from Lower Triassic strata from South Tibet. The sample positions are prefixed with a – sign or a + sign depending on the distance below or above the Permian-Triassic boundary that the sample was removed from. 1a-c, Ophiceras medium, Qubu section, +1.7 m; 2a-b, Gyronites sitala, Qubu section, +2.0 m; 3a-b, Japonites sp., Gongpu section, +6.3 m. Scale bar = 1 cm.

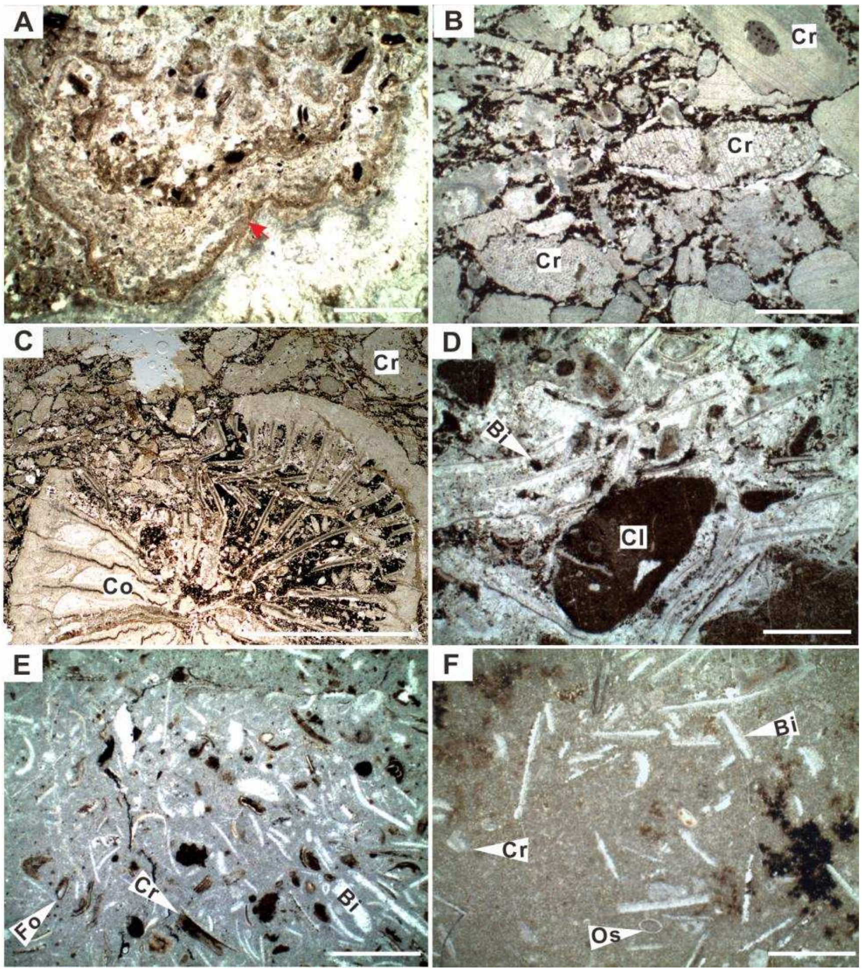

Fig. 4. Photomicrograghs of microfacies associations from inner to middle ramp settings. **(**A) Calcrete (MF1) with downward–growing, crust-like structure (red arrow) containing amorphous brown pigments, –0.15 m, Selong section. Scale bar = 1 mm. (B) Crinoid grainstone (MF2) exhibiting densely packed crinoid (Cr) fragments, –0.70 m, Selong section. Scale bar = 1 mm. (C) Coral-bearing grainstone containing slightly abraded rugose corals (Co) and abundant crinoid (Cr) fragments; the broken parts of corals are filled with crinoid fragments. –0.25 m, Selong section. Scale bar = 1 cm. (D) Shelly tempestite (MF4) consisting of densely-packed bivalve shells (Bi) with rounded micritic intraclasts (Cl), +0.30

m, Selong section. Scale bar = 1 mm. (E) Bioclastic packstone (MF5) containing abundant crinoid (Cr) and occasional bivalve (Bi) fragments and foraminifera (Fo), +1.25 m, Selong section. Scale bar = 1 mm. (F) Bioclastic wackestone containing diverse fossils (MF6), including bivalves (Bi), crinoids (Cr), and ostracods (Os), +1.8 m, Selong section. Scale bar = 1 mm.

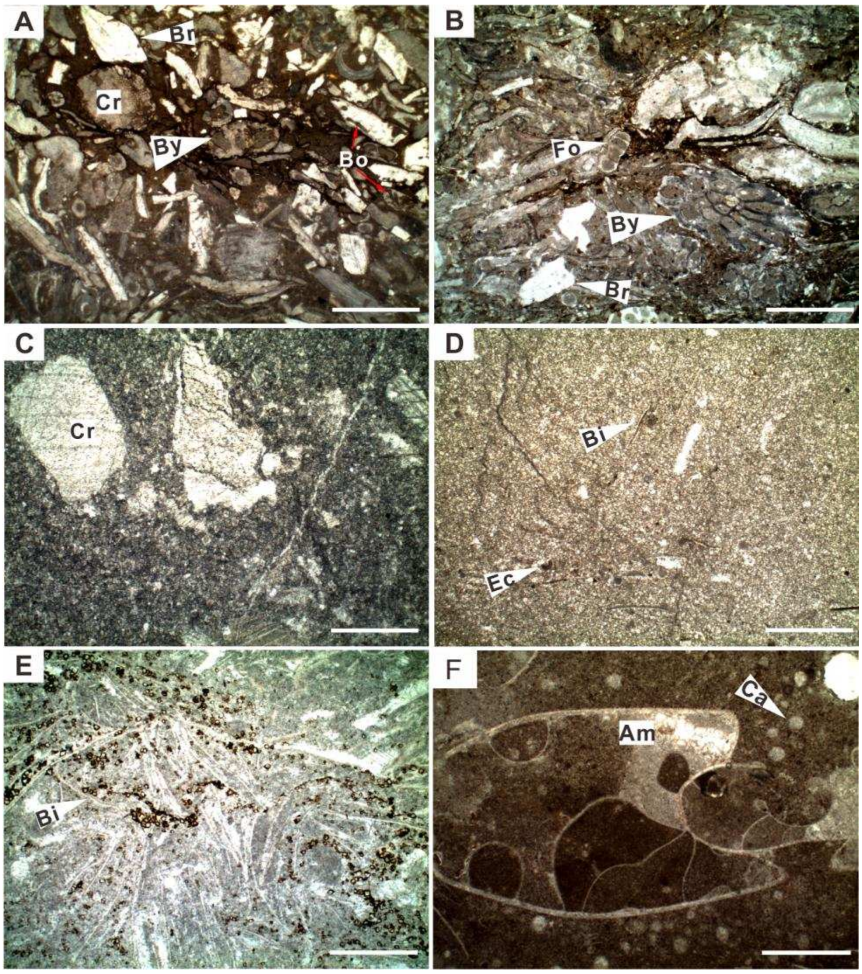

Fig. 5. Photomicrographs of microfacies associations from the outer ramp setting. (A) Bryozoan-echinoderm rudstone (MF7); note the abraded crinoids (Cr), brachiopod

fragments (Br) with micro-borings (Bo), and bryozoan fragments (By) showing relict fenestral structure, –4.50 m. Scale bar = 1 mm. (B) Bryozoan-echinoderm rudstone (MF7) containing bryozoans (By), small foraminifera (Fo) and brachiopod fragments (Br); note the well-preserved fenestral structure of bryozoans, –4.30 m. Scale bar = 1 mm. (C) Heavily abraded crinoid wackestone (MF8) consisting of occasional crinoid fragments (Cr) floating in micritic matrix, -0.6 m, Gongpu section. Scale bar = 1 mm. (D) Dolomitic bioclastic wackestone (MF9), which is made up of rare fragments of thin-shelled bivalves (Bi) and echinoderms (Ec) floating in a dolomicritic matrix, +1.8 m, Tulong section. Scale bar = 1 mm. (E) Thin-shelled bivalve packstone (MF10) consisting of thin-shelled bivalves with random orientations, +2.9 m, Tulong section. Scale bar = 1 mm. (F) Ammonoid-calcisphere wackestone (MF12), with a complete juvenile ammonoid (Am) and round, sparry calcispheres (Ca) floating in micritic matrix, +2.1 m, Qubu section. Scale bar = 1 mm.

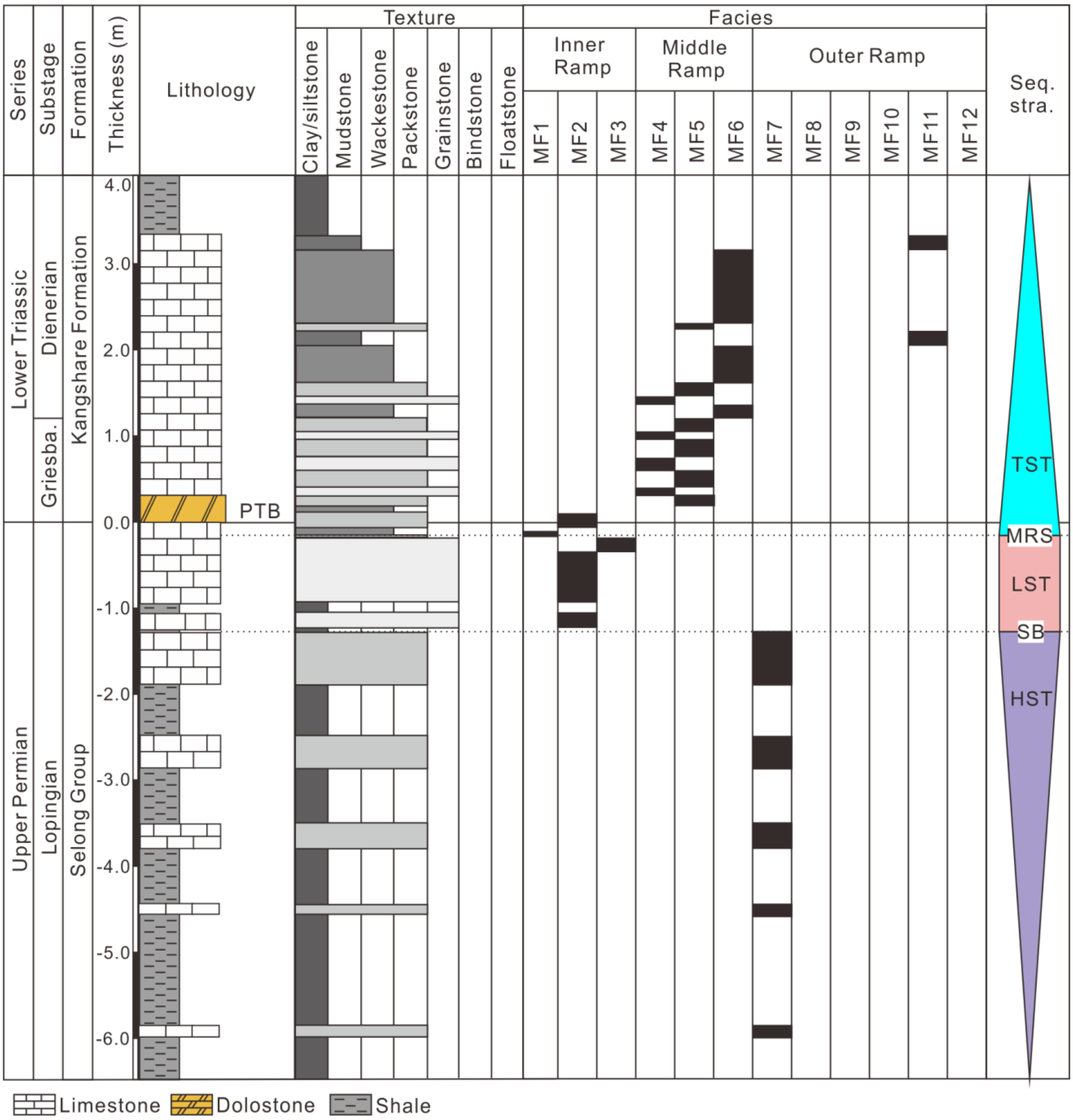

Fig. 6. Sequence stratigraphy and microfacies evolution from the uppermost Permian to the lowermost Triassic at the Selong section. 'Griesba.', Griesbachian. 'PTB', Permian-Triassic boundary. 'HST', highstand systems tract. 'LST', lowstand systems tract. 'TST', transgressive systems tract. 'SB', sequence boundary. 'MRS', maximum regression surface.

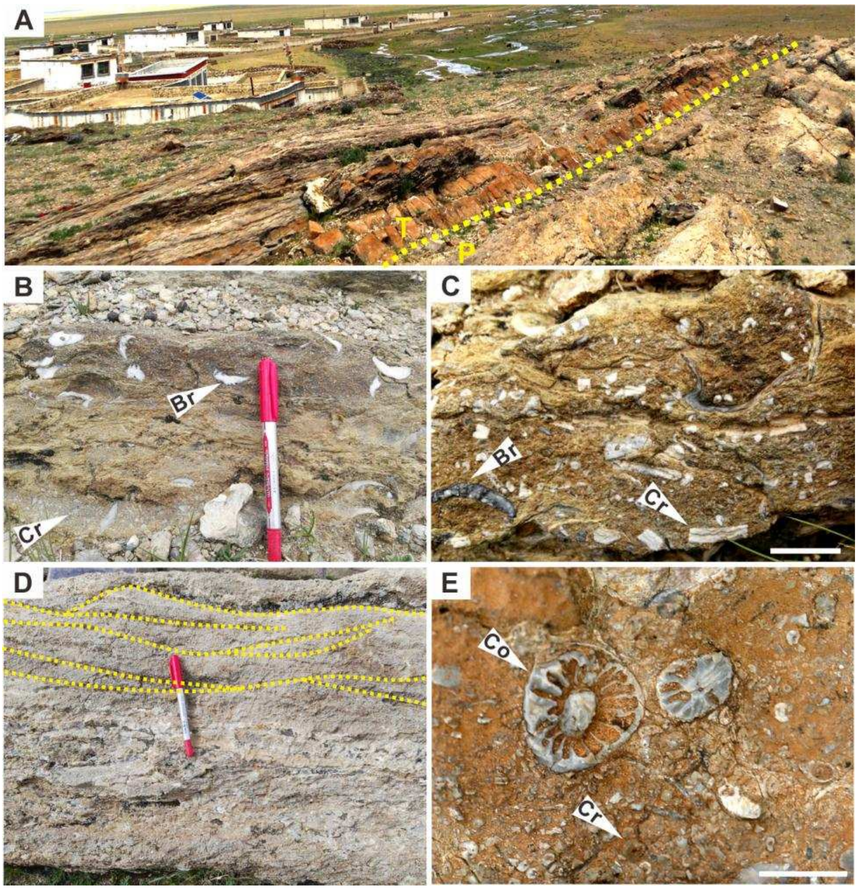

Fig. 7. (A) Field photos of macro-structures near the Permian-Triassic boundary at the Selong section, yellow dashed line marks the PTB. ‘P’, Permian; ‘T’, Triassic. (B) Thin-bedded, fossiliferous limestone containing abundant fragments of crinoids (Cr) and brachiopods (Br), –5.9 m. Pen (15 cm in length) for scale. (C) Bryozoan-echinoderm rudstone containing abundant fragments of bryozoans, crinoids (Cr) and brachiopods (Br), –4.5 m. Scale bar = 1 cm. (D) Crinoid grainstone showing cross-stratification (denoted by dashed lines) , –1.5 m. Pen (15 cm in length) for scale. (E) Coral-bearing grainstone that contains occasional corals (Co) floating in crinoid (Cr) grainstone, –0.25 m. Scale bar = 1 cm.

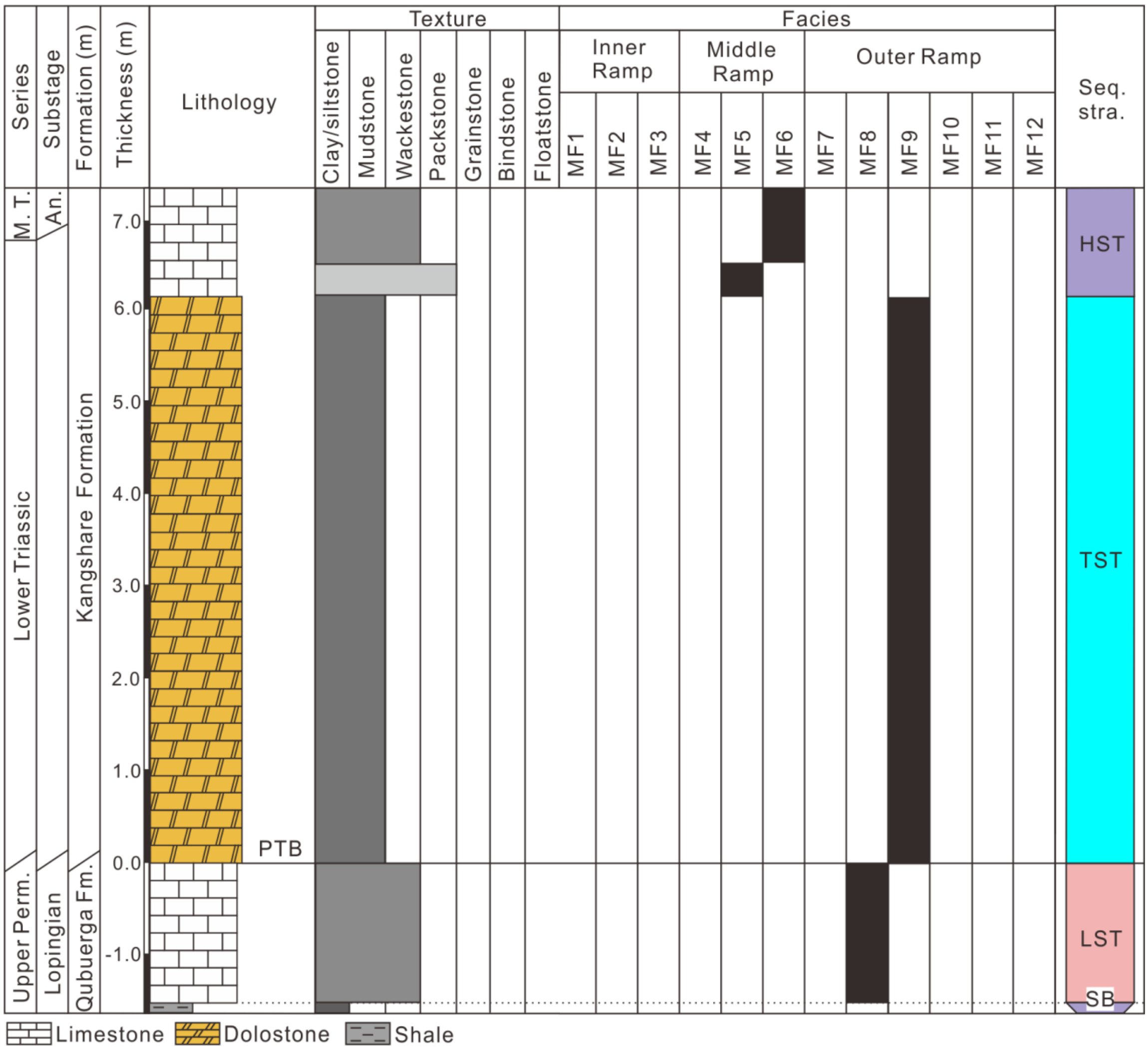

Fig. 8. Sequence stratigraphy and microfacies evolution from the uppermost Permian to the lowermost Triassic at the Gongpu section. ‘Perm.’, Permian; ‘M.T.’, Middle Triassic; ‘An.’, Anisian; ‘Fm.’, Formation. ‘PTB’, Permian-Triassic boundary. ‘LST’, lowstand systems tract. ‘TST’, transgressive systems tract. ‘SB’, sequence boundary. ‘HST’, highstand systems tract.

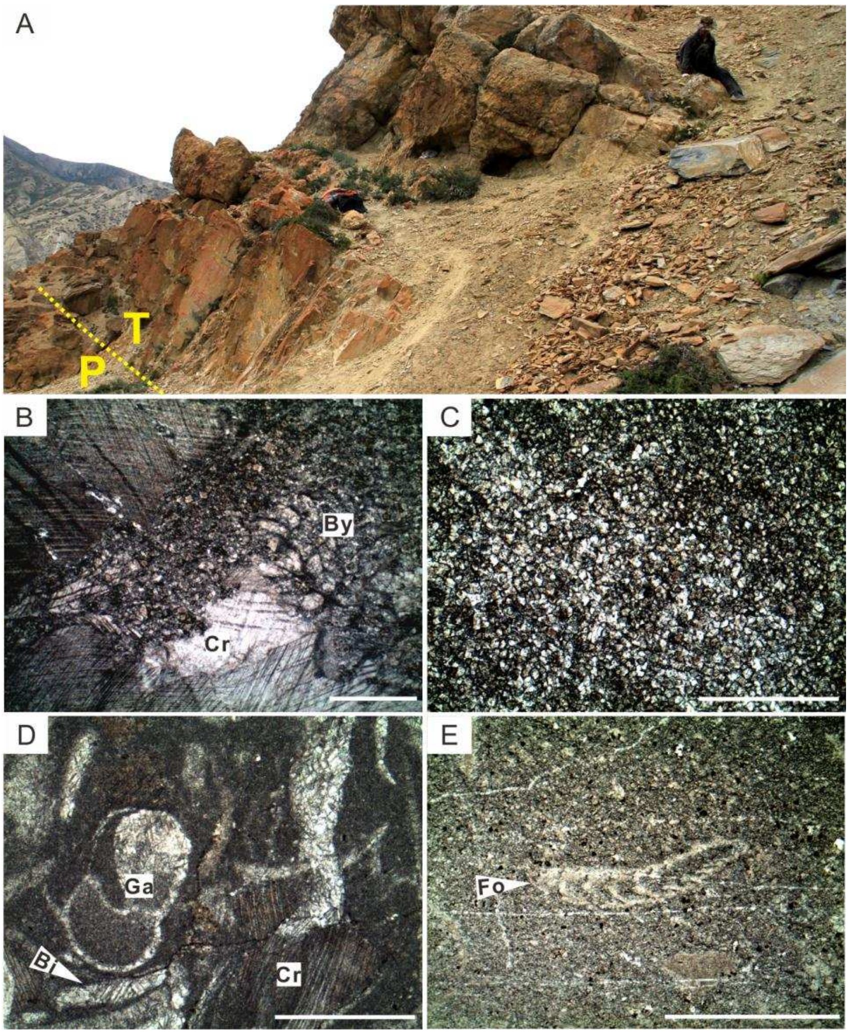

Fig. 9. (A) Field photograph of the Permian-Triassic boundary (PTB) at the Gongpu section, yellow dashed line marks the PTB. 'P', Permian; 'T', Triassic. (B) Bioclastic wackestone/mudstone consisting of highly abraded fragments of crinoids (Cr) (MF8) and bryozoans (By), –0.2 m. Scale bar = 1 mm. (C) Dolomitic mudstone (MF9) consisting of homogenous, fine (20-60 μm), subhedral to euhedral dolomite crystals, +2.0 m. Scale bar = 1 mm. (D) Bioclastic packstone (MF5) containing gastropods (Ga), bivalves (Bi), and crinoids (Cr), +6.2 m. Scale bar = 1 mm. (E) Bioclastic wackestone (MF6) containing the foraminifera Dentalina sp. (Fo), +6.6 m. Scale bar = 1 mm.

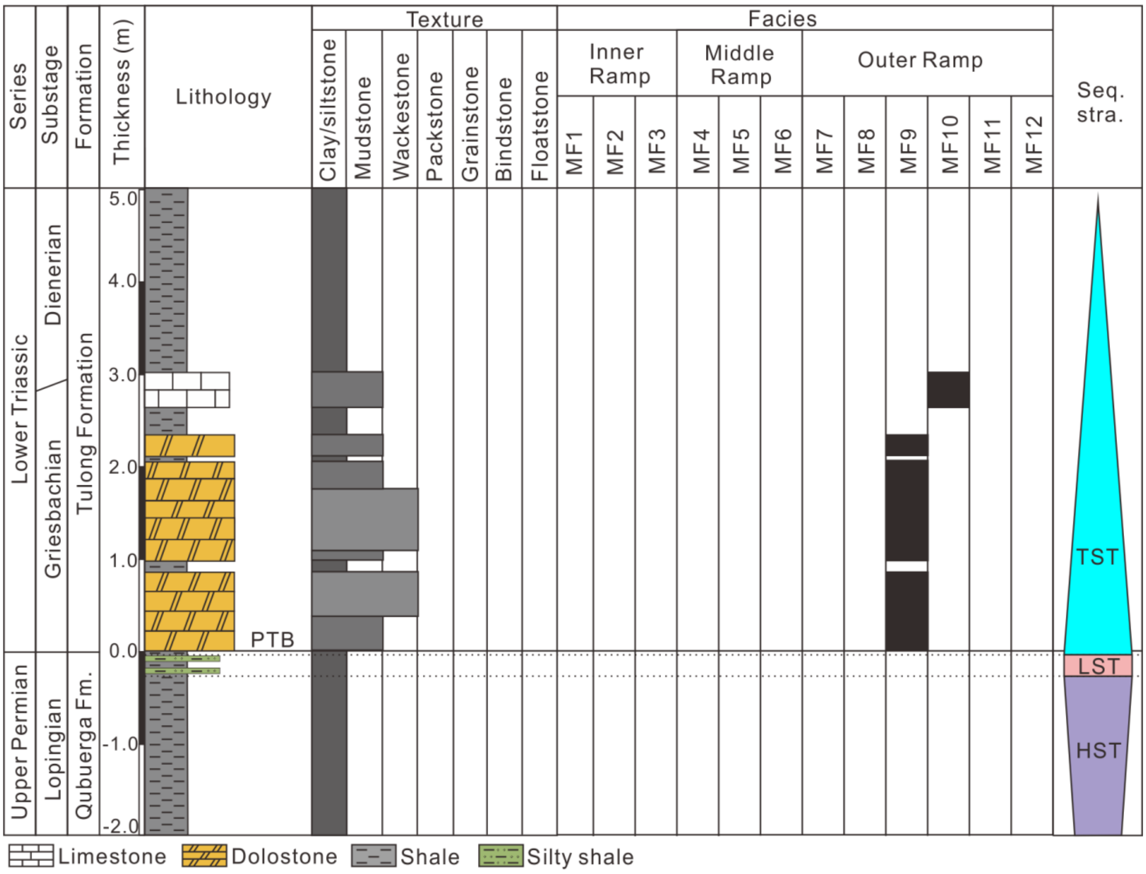

Fig. 10. Sequence stratigraphy and microfacies evolution from the uppermost Permian to the lowermost Triassic at the Tulong section. 'Fm.', Formation. 'PTB', Permian-Triassic boundary. 'HST', highstand systems tract. 'LST', lowstand systems tract. 'TST', transgressive systems tract.

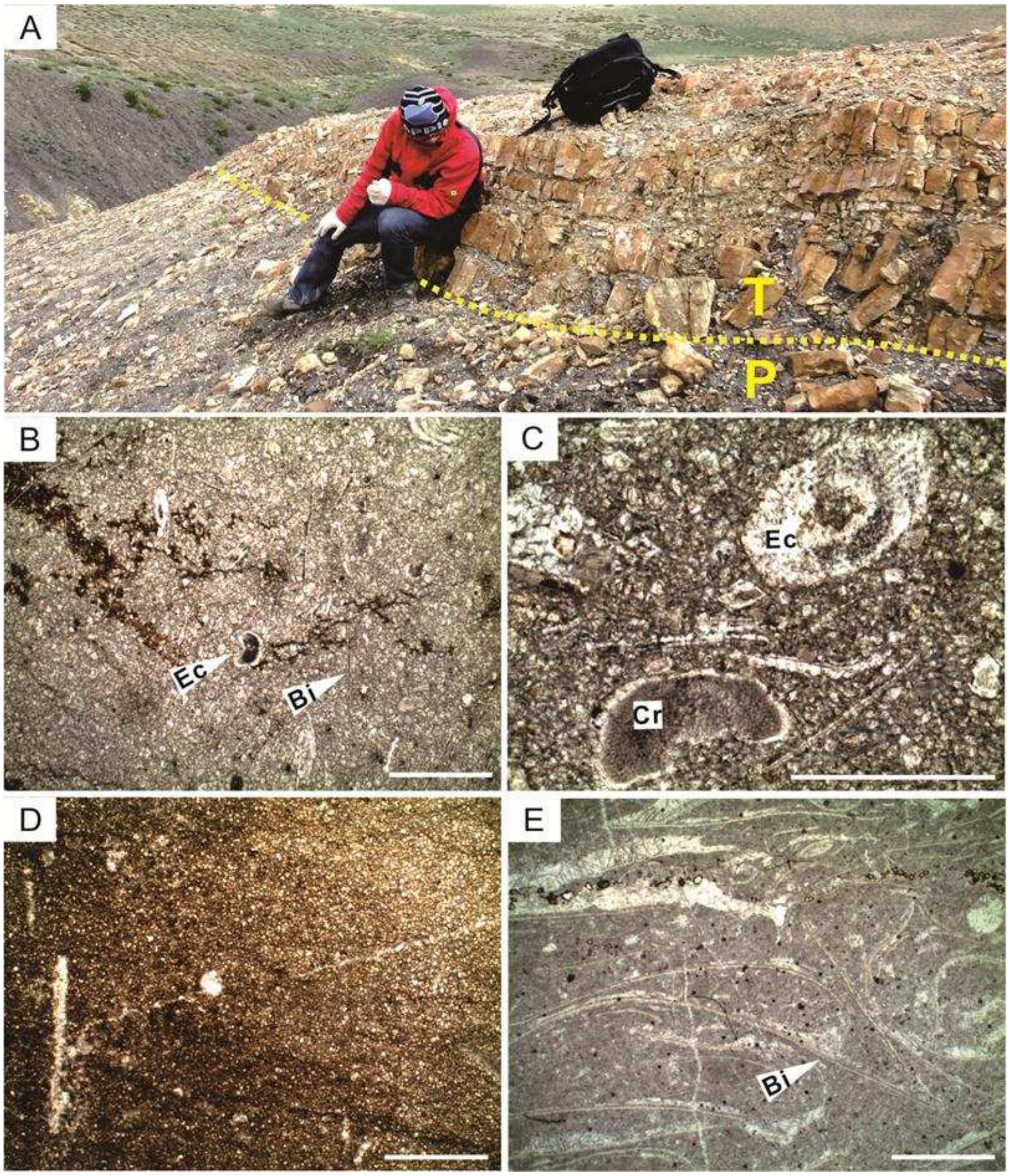

Fig. 11. (A) Field photograph of the Permian-Triassic boundary (PTB) at the Tulong section; yellow dashed line marks the PTB, ‘P’, Permian; ‘T’, Triassic. (B) Dolomitic bioclastic wackestone (MF9) containing rare echinoderm fragments (Ec) and thin-shelled bivalves (Bi), +0.5 m, scale bar = 1 mm. (C) Dolomitic bioclastic wackestone (MF9) containing an echinoid spine (Ec), and occasional crinoid fragments (Cr) floating in a matrix consisting of euhedral/subhedral dolomite crystals, +1.4 m, scale bar = 0.5 mm. (D) Dolomitic mudstone

(MF9) consisting of homogenous, fine (10-30 μm), subhedral to euhedral dolomite crystals, +2.3 m, scale bar = 1 mm. (E) Thin-shelled bivalve packstone (MF10) showing bivalve shells (Bi) with a random orientation, +2.9 m, scale bar = 1 mm.

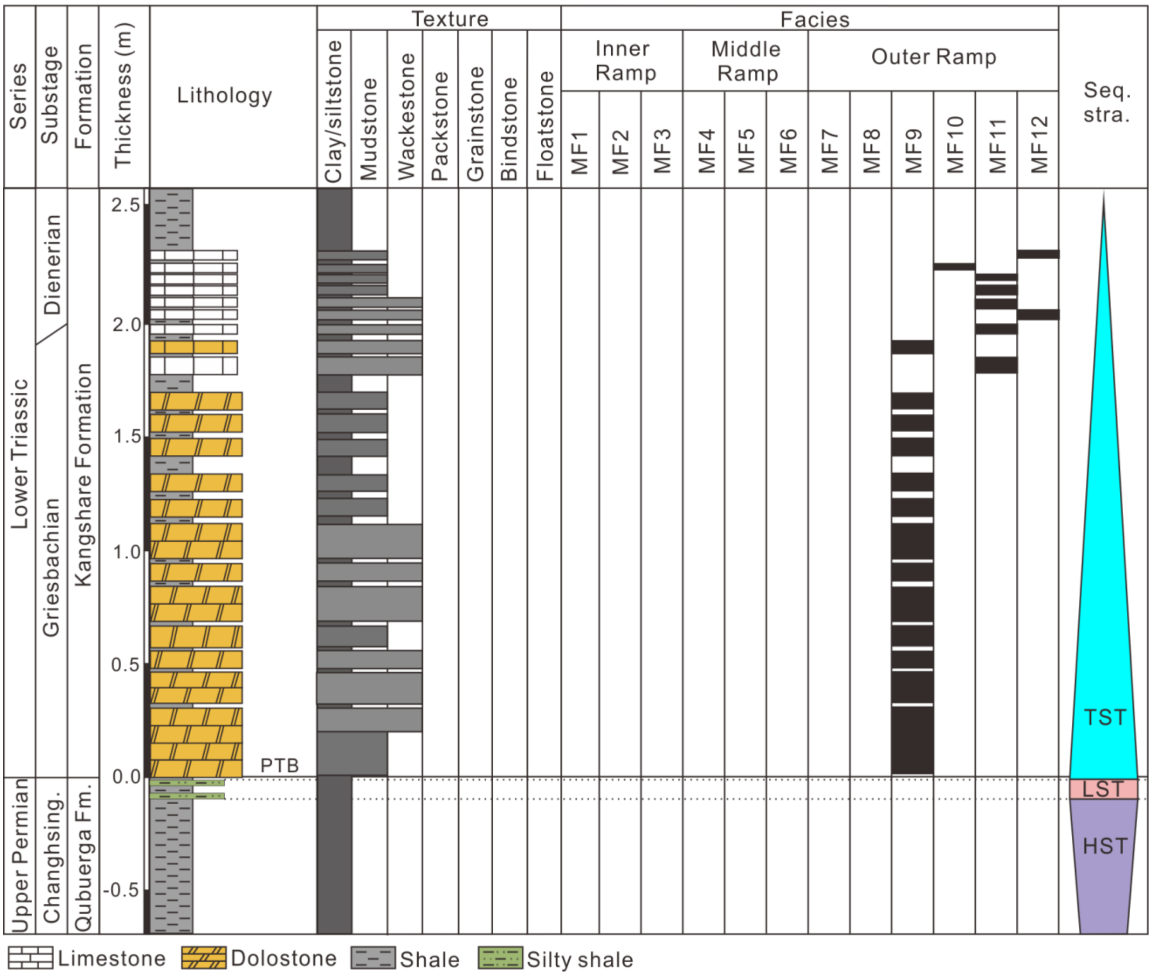

Fig. 12. Sequence stratigraphy and microfacies evolution from the uppermost Permian to the lowermost Triassic at the Qubu section. 'Changhsing.', Changhsingian; 'Fm.', Formation. 'PTB', Permian-Triassic boundary. 'HST', highstand systems tract. 'LST', lowstand systems tract. 'TST', transgressive systems tract.

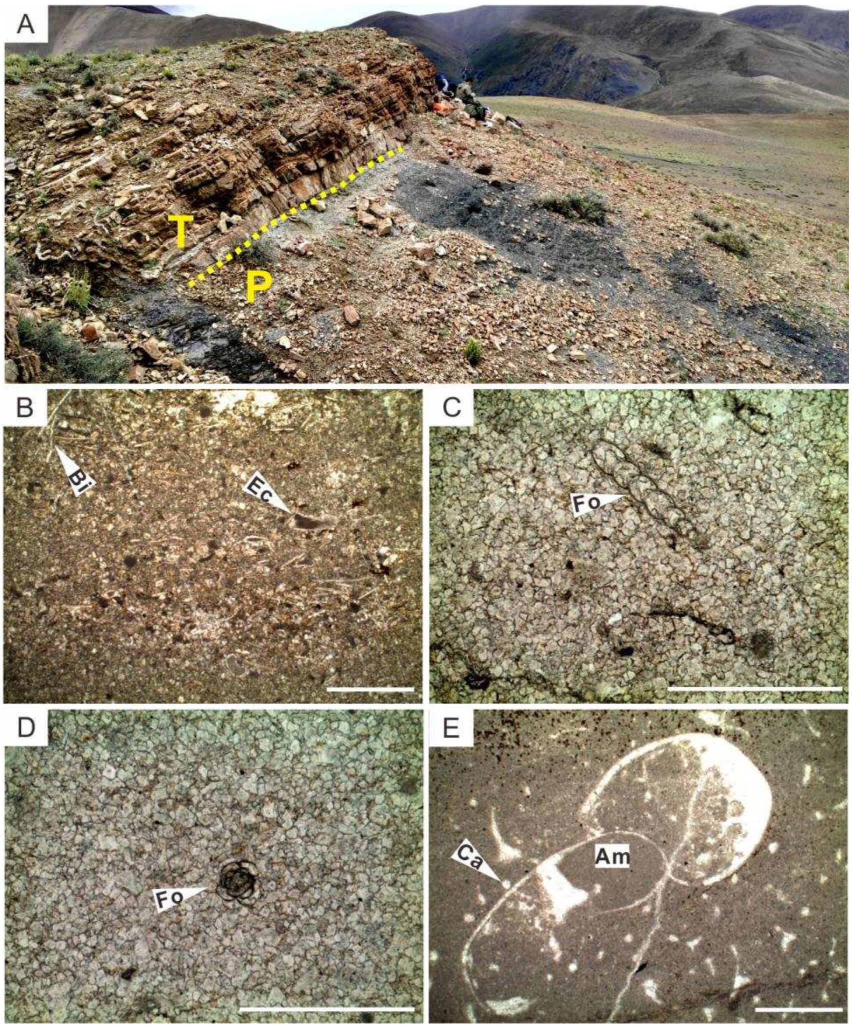

Fig. 13. (A) Field photograph of the Permian-Triassic boundary (PTB) at the Qubu section; yellow dashed line marks the PTB, ‘P’, Permian; ‘T’, Triassic. (B) Dolomitic bioclastic wackestone (MF9) containing rare echinoderm fragments (Ec) and thin-shelled bivalves (Bi), +0.4 m. Scale bar = 1 mm. (C) Dolomitic mudstone (MF9) consisting of homogenous, fine (20-50 μm in size) dolomite crystals, and the small foraminifera Nodosaria sp. (Fo), +0.2 m. Scale bar = 0.5 mm. (D) Dolomitic bioclastic wackestone (MF9) containing small foraminifera Glomospira sp. (Fo), +0.2 m. Scale bar = 0.5 mm. (E) Ammonoid-calcisphere wackestone (MF12) containing the occasional ammonoids (Am) and common calcispheres

(Ca), +2.7 m. Scale bar = 1 mm.

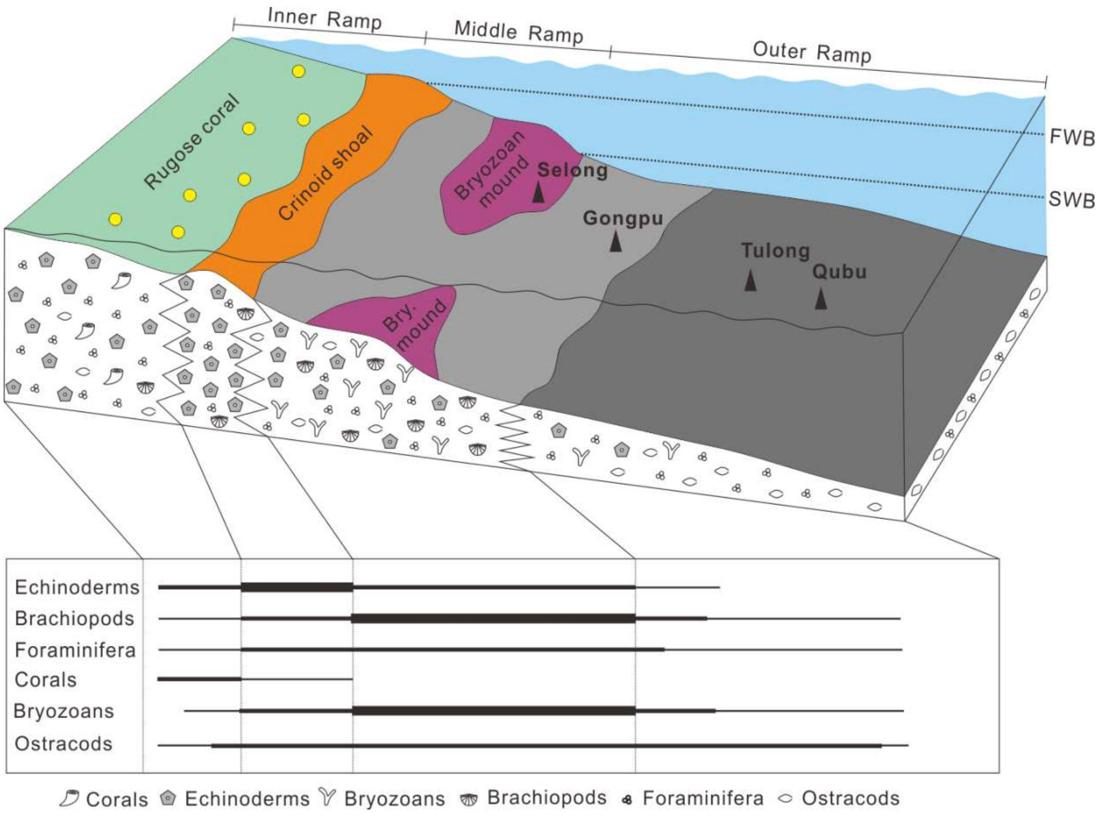

Fig. 14. Schematic carbonate sedimentary model for the latest Permian of South Tibet. The cool-water carbonate ramp is characterized by sporadically scattered rugose corals in the inner ramp and isolated patch mounds that are comprised of bryozoans and echinoderms in the middle to outer ramp. 'FWB', fair-weather wave base; 'SWB', storm wave base.

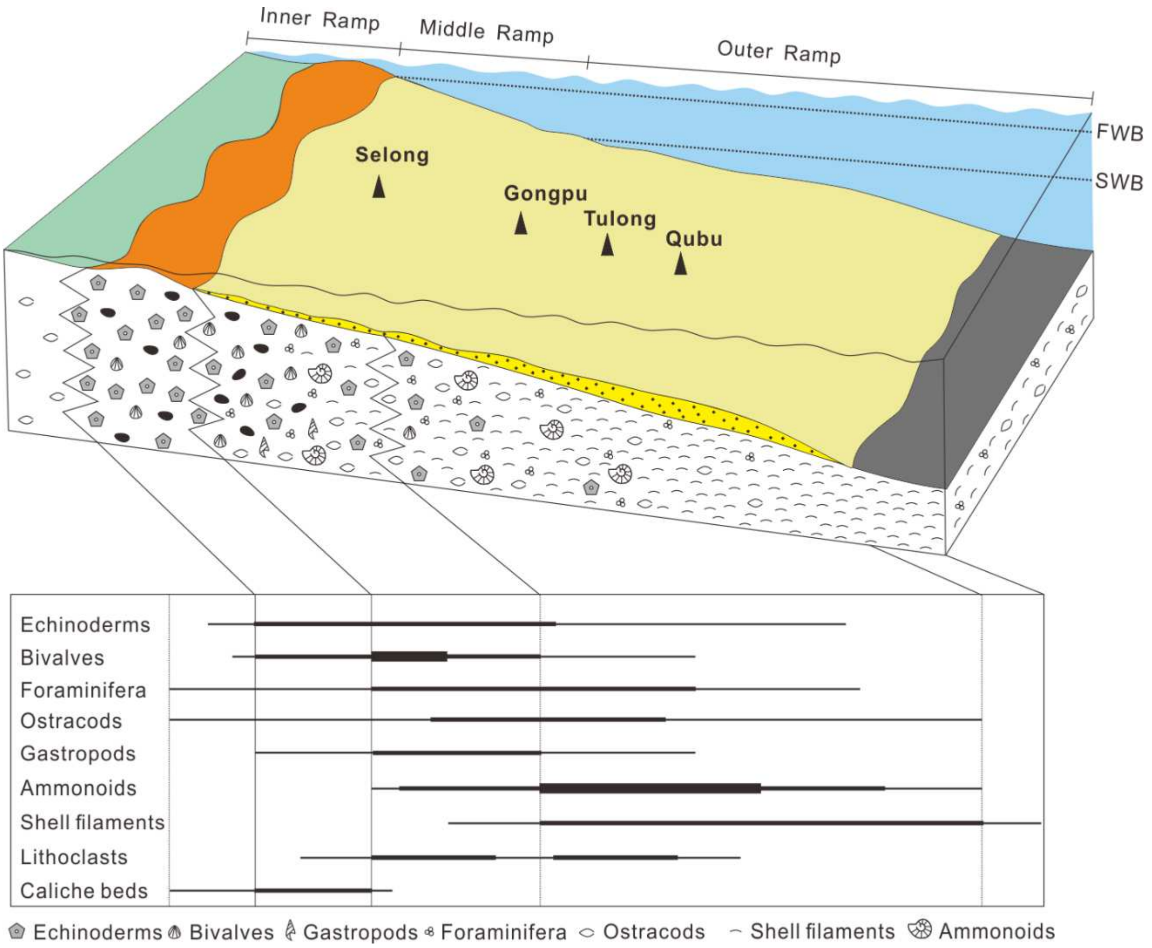

Fig. 15. Schematic carbonate sedimentary model for the earliest Triassic of South Tibet in the aftermath of the Permian-Triassic crisis. The homoclinal carbonate ramp is characterized by a shallow shoal comprised of bioclastic debris in the inner ramp and a gentle slope that consists of homogenous dolomitic lime mudstone in the middle to outer ramp. 'FWB', fair-weather wave base; 'SWB', storm wave base.

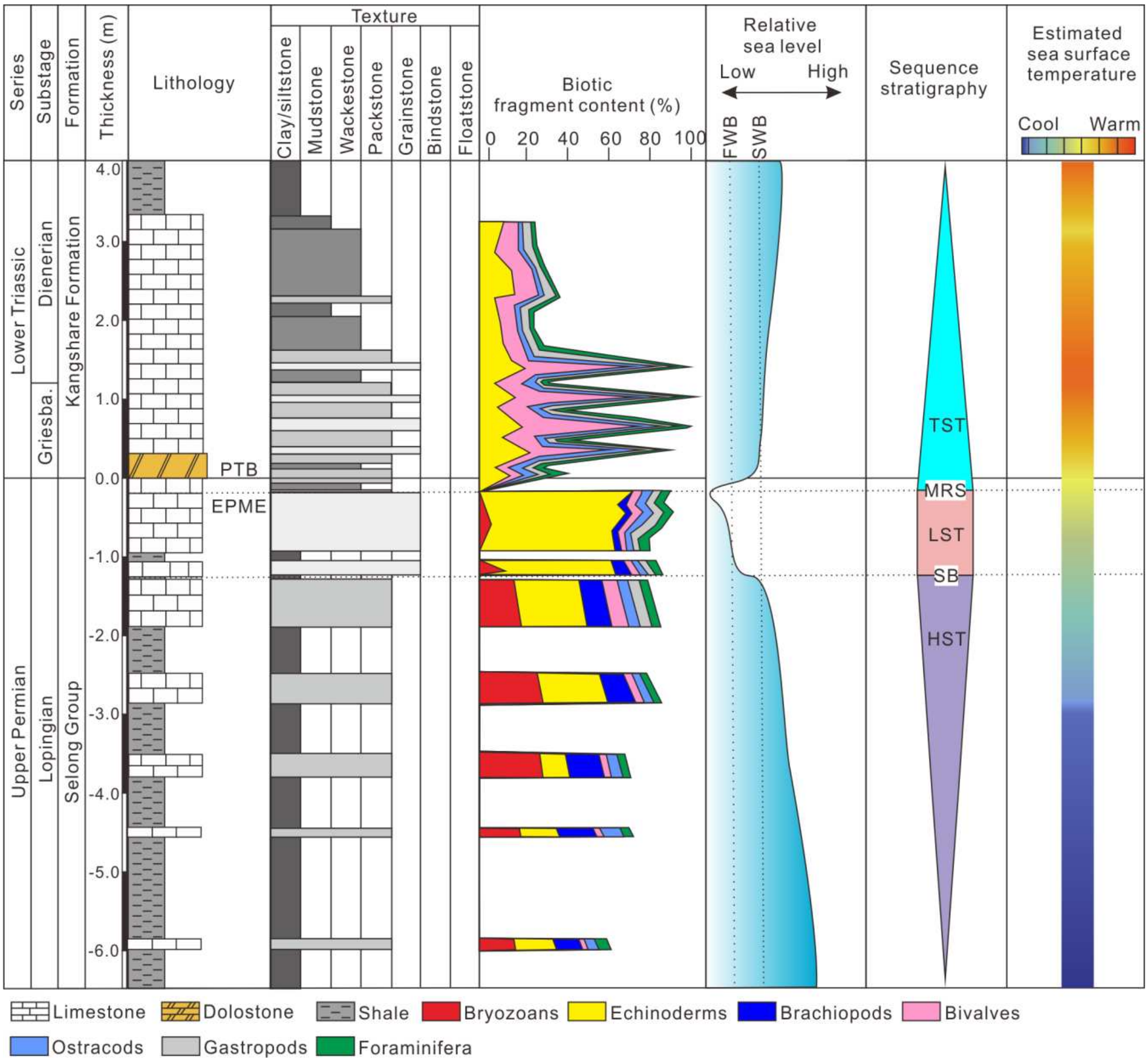

Fig. 16. Composite figure showing frequent changes in lithofacies, a sharp decrease in metazoan carbonate producing faunas, rapid sea level changes and significant global warming during the Permian-Triassic transition. Lithofacies and fossil data are from the Selong section. Estimated sea surface temperatures after Sun et al., (2012). 'FWB', fair-weather wave base; 'SWB', storm wave base. 'PTB', Permian-Triassic boundary. 'EPME', end-Permian mass extinction. 'HST', highstand systems tract. 'LST', lowstand systems tract. 'TST', transgressive systems tract. 'SB', sequence boundary. 'MRS',

maximum regression surface.

Table 1. Microfacies classification and description.

Microfacies	Biogenic content and texture	Sedimentary structure	Standard microfacies (Flügel, 2010)	Depositional setting
MF1 Calcrete	Minor peloids and rare ostracods; downward growth of laminated crusts.	mm-thick laminae	SMF26	
MF2 Crinoid grainstone	Abundant echinoderm fragments; minor foraminifera; grain-supported with sparite cement.	low angle cross-stratification	RMF27	Inner Ramp
MF3 Coral-bearing grainstone	Occasional corals floating in crinoid grainstone; slightly abraded corals filled with crinoid ossicles.	massive	RMF27	
MF4 Densely packed bivalve grainstone with micritic intraclasts	Abundant shell fragments with common, well-rounded intraclasts, rare ostracods and foraminifera; densely packed bivalves with sparry cement.	massive		
MF5 Bioclastic packstone with diverse fossils	Common echinoderm ossicles and bivalves with occasional ostracods, foraminifera and ammonoids; grain-supported with micritic matrix.	massive	RMF26	Middle Ramp
MF6 Bioclastic wackestone/floatstone	Minor bivalves, echinoderm ossicles, gastropods, ostracods and foraminifera; micritic matrix-supported.	massive or nodular bedding	RMF9	
MF7 Bryozoan-echinoderm rudstone	Abundant bryozoans, echinoderms, brachiopods and common foraminifera; grain-supported with micritic matrix; occasional micro-breccias.	massive	SMF5	Outer Ramp

MF8 Heavily abraded crinoid packstone/ wackestone	Dominated by echinoderm fragments with occasional bryozoan fragments; micritic matrix-supported; occasional micro-breccias.	massive	RMF9	
MF9 Dolomitic bioclastic wackestone/mudstone	Minor bivalves, echinoderms, ostracods, foraminifera, and calcispheres; micritic matrix-supported.	massive		
MF10 Thin-shelled bivalve packstone/ wackestone	Abundant thin-shelled bivalves with occasional juvenile ammonoids; sometimes densely packed.	massive	SMF3	Outer Ramp
MF11 Lime-mudstone	Pure micritic mudstone with common pyrite.	massive	RMF5	
MF12 Ammonoid-calcisphere wackestone	Occasional ammonoids with calcispheres; micritic matrix-supported.	massive	SMF8	